

1 **The Capability of Sentinel-MSI (2A/2B) and Landsat-OLI (8/9)** 2 **for Seagrass and Algae Species Differentiation using Spectral** 3 **Reflectance**

4 Abderrazak Bannari ¹, Thamer Salim Ali ² and Asma Abahussain ²

5 ¹Space Pix-Map International Inc., Gatineau (Québec) J8R 3R7, Canada

6 ²Department of Natural Resources and Environment, College of Graduate Studies, Arabian Gulf University, Manama,
7 Kingdom of Bahrain, P.O. Box: 26671, Tel: (973) 1723-9545; Fax: (973) 1723-9552.

8
9 Correspondence to: Abderrazak Bannari, Email: abannari@bell.net

10
11 **Abstract.** This paper assesses the reflectance difference values between the homologous visible and near-infrared
12 (VNIR) spectral bands of Sentinel-MSI-2A/2B and Landsat-OLI-8/9 sensors for seagrass, algae, and mixed species
13 discrimination and monitoring in a shallow marine environment southeastern of Bahrain in the Arabian Gulf. To
14 achieve these, a field survey was conducted to collect samples of seawater, underwater sediments, seagrass (*Halodule*
15 *uninervis* and *Halophila stipulacea*) and algae (green and brown). As well, an experimental mode was established in
16 a Goniometric-Laboratory to simulate the marine environment, and spectral measurements were performed using an
17 ASD spectroradiometer. Measured spectra and their transformation using continuum-removed reflectance spectral
18 (CRRS) approach were analyzed to assess spectral separability among separate or mixed species at varying coverage
19 rates. Afterward, the spectra were resampled and convolved in the solar-reflective spectral bands of MSI and OLI
20 sensors and converted into water vegetation indices (WVI) to investigate the potential of red, green, and blue bands
21 for seagrass and algae species discrimination. The results of spectral and CRRS analyses highlighted the importance
22 of the blue, green, and NIR wavelengths for seagrass and algae detection and likely discrimination based on
23 hyperspectral measurements. However, when resampled and convolved in MSI and OLI bands, spectral information
24 loses the specific and unique absorption features and becomes more generalized and less precise. Therefore, relying
25 on the multispectral bandwidth of MSI and OLI sensors is difficult or even impossible to differentiate or to map
26 seagrass and algae individually at the species level. Instead of the red band, the integration of the blue or the green
27 bands in WVI increases their discriminating power of submerged aquatic vegetation (SAV), particularly WAVI,
28 WEVI, and WTDVI indices. These results corroborate the spectral and the CRRS analyses. However, despite the
29 power of blue wavelength to penetrate deeper into the water, it also leads to a relative overestimation of dense SAV
30 coverage due to the higher scattering in this part of the spectrum. Furthermore, statistical fits ($p < 0.05$) between the
31 reflectance in the VNIR homologous bands of SMI and OLI revealed excellent linear relationships (R^2 of 0.999) with
32 insignificant RMSD (≤ 0.0015). Important agreements ($0.63 \leq R^2 \leq 0.96$) were also obtained between homologous
33 WVI regardless of the integrated spectral bands (i.e., red, green, and blue), yielding insignificant RMSD (≤ 0.01).
34 Accordingly, these results pointed out that MSI and OLI sensors are spectrally similar, and their data can be used
35 jointly to monitor accurately the spatial distribution of SAV and its dynamic in time and space in shallow marine
36 environment, provided that rigorous data pre-processing issues are addressed.

37 1. Introduction

38 Seagrass meadows are identified as an important key for the characterization of environmental resources in estuarine
39 and shallow coastal areas, and a fundamental health index allowing the assessment of coastal ecosystems. The
40 composition and density of their species depend largely on water depth, temperature, salinity, coastal substrate
41 material, and light penetration (Dierssen et al., 2015). Adapted to grow in shallow seawater down to a depth of 20 m,
42 where approximately only 11% of surface light reaches the bottom (Duarte and Gattuso, 2008), they play an essential
43 role in the sustainability of global ecosystem biodiversity in most shallow near-shore areas around the world (Den-
44 Hartog, 1970; Konstantinos *et al.*, 2016). Moreover, the biodiversity of seagrass provides secure habitat and food for
45 a wide variety of marine micro-organisms, improve the quality of water and protect shorelines against erosion in the
46 middle and lower intertidal and sub-tidal zones (Roelfsema *et al.*, 2009; Anders and Lina, 2011; Yang and Yang,
47 2012; Morrison *et al.*, 2014). Like other vegetation cover, seagrass beds play an important role in carbon storage
48 (Novak and Short, 2020), as well as effective removal of carbon dioxide from the “biosphere-atmosphere” system,
49 which significantly mitigates the climate change impacts (Duarte et al., 2013; Lyimo, 2016). Although occupying only
50 0.2% of the world’s oceans (Traganos, 2020), seagrass beds can store twice as much as forests, and sequester around
51 10% of the total carbon received by the oceans (Fourqurean et al., 2012).

52 Unfortunately, natural and anthropogenic disturbances and disasters have led to the decline of seagrass around the
53 world (Green and Short, 2003; Orth et al., 2006; Grech et al., 2012; Wood, 2012) at local and regional scales.
54 Undoubtedly, these causes substantially destroy the seagrass beds and biota associated in such habitat and unbalance
55 the ecological functions of coastal zones. Short et al. (2011) showed that seagrass habitat disappeared worldwide at a
56 rate of 110 km² per year between 1980 and 2006. Hence, understanding the spatial distribution of seagrass biomass,
57 its extent, condition, and change over time is essential for their monitoring, management, and protection (Short and
58 Coles, 2001; Waycott *et al.*, 2009). Such monitoring provides updated and accurate information useful for the
59 protection of several ecosystems (Leleu et al., 2012), conservation (Hamel and Andréfouët, 2010), coastal risk
60 assessment (Warren et al., 2016), ecological resources development (Boström et al., 2011), and marine spatial
61 planning (Saarman et al., 2012; Kibele, 2017). In addition, mapping and inventorying the total aboveground biomass
62 of seagrass and algae are important for ecosystem health assessment (Short and Wyllie-Echeverria, 1996), alteration
63 and dynamics in space-time (Neckles et al., 2012), biomass productivity and its contribution to the global biosphere
64 carbon sink capacity (Waycott et al., 2009), and understanding the impacts of climate change (Hashim et al., 2014).

65 In the Arabian Gulf, the extreme environmental conditions combined with major seasonal variations in the marine
66 environment promote the development of three seagrass species including *Halodule uninervis* which is the most
67 dominant species, *Halophila stipulacea* that is less common, and *Halophila ovalis*, which is widely scattered and
68 rarely forms relatively dense meadows. Along the western coast of the Arabian Gulf, these three species are reported
69 and several species of marine algae are described, especially green and brown algae (Erfteimeijer and Shuail, 2012).
70 This natural resource is located in shallow waters with depths ranging from the intertidal zone to 20 m, supporting the
71 second largest population of dugongs (*Dugong dugon*) in the world (Preen, 2004); as well as a large population of
72 Green Turtles (*Chelonia mydas*) and Hawksbill Turtles (*Eretmochelys imbricata*) (Thakur et al., 2007). Unfortunately,
73 these coastal ecosystems are under continuous threats from anthropogenic activities (Waycott et al., 2009), such as

74 reclamation and dredging where several coastal developmental projects are constructed and others under construction
75 (small islands projects development), industrial effluents, oil exploration, pipeline laying, maritime transportation,
76 intensive circulation of commercial fishing boats, pollution and discharges of seawater desalinization and wastewater
77 into the sea (Onuf, 1994; Dunton and Schonberg, 2002; Burfeind and Stunz, 2006; Naser, 2011; Erfteimeijer and
78 Shuail, 2012). Eventually, these activities catalyze the degradation and destruction of seagrass species and related
79 ecosystems. Therefore, the assessment of seagrass conditions associated with broad scale of benthic species should be
80 based on relevant and accurate information to measure several health indicators of coastal areas to ensure the
81 sustainable development of these natural resources.

82 Previously, photo-interpretation approaches based on aerial photography have been adopted to follow seagrass and
83 algae species development and assessment in space and time (Ferguson and Wood, 1990; Meehan et al., 2005; Mount,
84 2007). Afterward, the first generation of satellite remote sensing was used to investigate the seagrass classes'
85 composition, differentiation, classification, etc. (Hossain et al., 2014; Komatsu et al., 2020). Unfortunately, these goals
86 were difficult to achieve accurately because the radiometric and spectral resolutions of sensors lacked the sensitivity
87 to discriminate among different marine vegetation species and fragmented classes (Mumby et al., 1997; Wicaksono
88 and Hafizt, 2013). To improve land-water surfaces reflectivity and information extraction, recent developments in
89 remote sensing science and technology have led to an improvement of sensors performance in spatial and spectral
90 resolutions, assuming a potential mapping of the marine environment and aquatic vegetation at the species level;
91 obviously, if species under investigation have distinct spectral signatures. For instance, the Multi-Spectral Instruments
92 (MSI) onboard Sentinel 2A and 2B, as well as the Operational Land Imager (OLI) sensors onboard Landsat 8 and 9
93 platforms were designed with a significant improvement of the signal-to-noise ratio (SNR) and radiometric
94 performances (Knight and Kvaran, 2014). The availability of this new generation of sensors offers innovative
95 opportunities for long-term high-temporal frequency for Earth surfaces' observation and monitoring (Mandanici and
96 Bitelli, 2016). The free availability of their data significantly advances the applications of remote sensing with medium
97 spatial resolutions (Roy et al., 2014; Wulder et al., 2015; Zhang et al., 2018). Thanks to the improvement of their
98 spectral, radiometric, and temporal resolutions, they can expand the range of their applications to several natural
99 resources and environmental domains for monitoring, assessing, and investigating (Hedley et al., 2012a and 2012b).
100 Moreover, the orbits of these four satellites constellation are designed to ensure a revisiting interval time of less than
101 2 days (Li and Roy, 2017; Li and Chen, 2020), thereby substantially increasing the monitoring capabilities of the
102 Earth's surface and ecosystems (Drusch et al., 2012). Their spectral resolutions and configurations are designed in
103 such a way that there is a significant match between the homologous spectral bands, i.e. analogous manner for relative
104 spectral filters position and bandwidths between bands (Drusch et al., 2012; Irons et al., 2012). However, depending
105 on the sensitivity of the intended application (Flood, 2017), the sensor radiometric drift calibration (Markham et al.,
106 2016), the atmospheric corrections (Vermote et al., 2016), the surface reflectance anisotropy (Roy et al., 2017), and
107 the sensors co-registration (Skakun et al., 2017; Yan et al., 2018), it is plausible that the natural surface-reflectances
108 recorded by MSI and OLI sensors over the same target in the marine environment may be different. In addition, the
109 relative spectral response profiles characterizing the filters (spectral responsivities) of these instruments are not
110 perfectly identical between the homologous bands, so some differences are probably expected over the recorded land

111 or water surfaces reflectance values and, therefore, their data cannot be reliably used together (Bannari et al., 2004;
112 Van-derWerff and Van-der-Meer, 2016; Bannari, 2019). The importance of these differences depends on the
113 application (spectral characteristics of the observed target) and on the approach adopted to perform time-series
114 analyses, mapping, or change detection exploiting these instruments (Flood, 2017). For instance, it is plausible that
115 the extraction of seagrass and/or algae information in time over shallow water areas using surface reflectances,
116 empirical, semi-empirical, and/or physical approaches, may affect the comparison of the results.

117 The main objectives of this research focus on the analysis of Sentinel-MSI and Landsat-OLI homologous visible
118 and near-infrared (VNIR) bands capability to distinguish and discriminate among seagrass (*Halodule uninervis* and
119 *Halophila stipulacea*), algae (green and brown), and any probable case of mixed species of seagrass and algae sampled
120 from the southeast area of Bahrain national water. To achieve these, the specific following steps are considered. 1)
121 Examination of spectral signatures in VNIR wavelengths and their continuum-removal transformations for potential
122 differentiation among the considered seagrass and algae species and their mixture submerged in seawater at different
123 coverage rates, as well as considering the sediment-substrate with clear and dark colors. 2) Comparison and analysis
124 of the difference between the resampled and convolved reflectances in the VNIR homologous bands of MSI and OLI
125 sensors considering all examined samples. 3) Comparison between MSI and OLI sensors in terms of converting the
126 reflectances over the considered samples at different coverage rates into several water vegetation indices (WVI).
127 Finally, 4) efficiency and accuracy analysis of the examined WVI to discriminate between species (seagrass, algae
128 and mixed) by integrating the green and blue bands instead of the red band. Further, according to these analyses
129 results, it will be clear whether it possible for these sensors to differentiate between seagrass and algae effectively and
130 precisely at the species level, or simply and generally to discriminate among submerged aquatic vegetation (SAV)
131 cover at different density classes.

132 **2. Remote sensing of seagrass and algae detection and mapping: A review**

133 Traditional seagrass *in-situ* surveys require time and intensive field sampling, which is generally lack the spatial
134 coverage and precision that are required to detect changes before they become irreversible or very difficult to maintain
135 year after year (Peterson and Fourqurean, 2001; Yang and Yang, 2012). Over the recent decades, remote sensing
136 science and sensors technology has played an essential role in seagrass mapping and monitoring (Dean and Salim,
137 2013; Dierssen et al., 2015). According to literature, the mapping of the characteristics and properties of seagrass and
138 algae in the marine environment occurs over relatively small areas with limited variations in water depth and clarity
139 using satellite, airborne, and drone remote sensing sensors (multispectral and hyperspectral). Moreover, field and
140 laboratory *in-situ* measurements have been conducted for calibration and validation in several environments around
141 the world (Larkum *et al.*, 2006; Roelfsema *et al.*, 2009; Hossain et al., 2014; Komatsu et al., 2020; Duffy et al. 2018).

142 Under laboratory conditions using spectral measurements, Thorhaug *et al.* (2007) demonstrated the near similarity
143 in the shape and form of the spectral signatures of three different seagrass species with a very slight difference and
144 pointed out subtle differences between marine algae (green and brown) and seagrass. In the central west coast of
145 Florida in the USA, Pu *et al.* (2012) used *in-situ* Hyperspectral measurements in the field and laboratory to analyse
146 the spectral behaviour and the potential discrimination among several seagrass species according to their spatial extent

147 and abundance, water depths, and substrate types. They highlighted that the discrimination of seagrass species and the
148 percentage of SAV coverage are affected by water depth and substrate on the measured spectra. Moreover, Wood
149 (2012) demonstrated the potential of the synergy between the field spectra and hyperspectral data for seagrass sensing
150 and mapping in Redfish Bay, Texas in the USA. Exploiting modeled and simulated data, Hedley *et al.* (2012a)
151 demonstrated that Sentinel-MSI has an improved capability for detection and discrimination of the marine
152 environment compared to SPOT-4 and Landsat-ETM+. Furthermore, Fyfe (2003) reported that the spectral signatures
153 measured on harvested wet leaves (out of water) of different seagrass species were spectrally distinct. However, the
154 real marine environment conditions are different from wet leaves due to water-column constituents including
155 phytoplankton, suspended organic and inorganic matter, water depth variability, and optical properties of the
156 underlying sediments (Pu *et al.*, 2012).

157 Otherwise, NASA's Landsat program is the earliest and most commonly used over the past five decades. It consists
158 of a series of nine satellite missions using four types of multispectral sensors including MSS, TM, ETM +, and OLI
159 (Bannari and Al-Ali, 2020). These sensors have been used by many scientists to detect and map seagrass beds at local
160 and regional scales (Phinn *et al.* 2008; Knudby and Nordlund, 2011; Lyons *et al.* 2012 and 2013; Kovacs *et al.* 2018).
161 Exploring a time-series of 23 annual images acquired over the Eastern Banks of Moreton Bay in Australia, Lyons *et al.*
162 (2013) demonstrated how TM and ETM+ data time-series analysis enabled seagrass spatial distribution to be
163 appropriately assessed spatiotemporally. Moreover, a regional-scale mapping of seagrass habitat in the Wider-
164 Caribbean region was achieved with acceptable accuracies using a total of 40 scenes acquired with TM and ETM+
165 sensors, and applying different images processing methods (Wabnitz *et al.*, 2008). In Cam-Ranh Bay in Vietnam,
166 Chen *et al.* (2016) investigated the temporal changes of seagrass beds over 20 years (1996 to 2015) by exploiting
167 multi-temporal Landsat data acquired with TM, ETM+ and OLI sensors. Dekker *et al.* (2005) demonstrated that TM
168 and ETM+ instruments did not have sufficient spectral and radiometric resolutions to discriminate among three
169 seagrass species in a shallow coastal Australian lake. Contrariwise, Dahdouh-Guebas *et al.* (1999) reported the utility
170 of TM data associated with ground truth measurements to map accurately the distribution of seagrass and algae on the
171 Kenyan coast. In addition to the Landsat sensor series, the European satellites such as SPOT-HRV were also used in
172 combination with *in-situ* spectroradiometric measurements and quantitative semi-empirical models to assess the
173 changes in the spatial distribution of seagrass biomass in Bourgneuf-Bay in France over 14 years (Barillé *et al.* 2010).
174 Likewise, the potential of the Indian satellite (IRS-ID LISS-III) has been demonstrated for mapping the seagrass
175 meadows extent in the Gulf of Mannar Biosphere Reserve in India (Umamaheswari *et al.*, 2009).

176 Furthermore, the first generation of commercial satellites operated by the private remote sensing industry with
177 very high pixel size and narrow spectral resolutions, such as IKONOS, Quickbird, WorldView, etc., offers
178 complementary technology for seagrass sensing and mapping. This new technology provides an excellent compromise
179 between spatial and spectral resolutions for information extraction. In clear water seagrass habitat in the Moreton-Bay
180 (Australia), the spatial and temporal dynamics of seagrasses (cover, species, and biomass) have been studied from the
181 leaf to patch scales between 2004 and 2013 integrating nine high spatial resolutions images acquired with WorldView-
182 2, IKONOS, and Quickbird-2 and applying object-image processing approach (Roelfsema *et al.*, 2014). The results
183 showed the utility of this new spatial technology for time-series analysis and the derivation of seagrass products that

184 are very useful in marine ecology management. Moreover, Knudby and Nordlund (2011) highlighted the utility of
185 IKONOS data for multi-species of seagrass detection in a patchy environment around Chumbe Island in Zanzibar
186 (Tanzania). Along Zakynthos Island in Greece, Pasqualini *et al.* (2005) demonstrated that the SPOT-5 data with 2.5
187 and 10 m spatial resolutions are suitable for seagrass classes' classification according to the overall accuracies. In
188 shallow waters of Moreton Bay in Australia, Phinn *et al.* (2008) have shown that the spatial and spectral resolutions
189 of multispectral (Quickbird and Landsat-TM) and hyperspectral (airborne CASI) data affects the precision of seagrass
190 biomass differentiation at the species level, i.e., when the pixel size increases the error is getting higher. Contrary to
191 these findings, in the Capo Rizzuto area in Italy, Dattola *et al.* (2018) reported the potential of the high spatial
192 resolution of WorldView-2 compared to the medium resolution of MSI and OLI for different seagrass species
193 characterization. In addition, to identify the spatial distribution of seagrass beds in Xincun Bay (Hainan province in
194 China), Yang and Yang (2009) demonstrated that Quickbird data are more accurate than those of TM and CBERS
195 (China-Brazil Earth Resources Satellite data) sensors.

196 In addition to remote sensing sensor technologies, a variety of image processing methods have been employed in
197 mapping seagrass spatial distribution and coverage. For instance, Marcello *et al.* (2018) demonstrated the good
198 performance of support vector machines (SVM) approach compared to spectral angle mapper (SAM) and maximum
199 likelihood for seagrass classification; moreover, they pointed out the greater aptitude of hyperspectral compared to
200 multispectral data. Likewise, Peneva *et al.* (2008) reported that the maximum likelihood classification produced the
201 highest overall accuracy while SAM yielded the lowest accuracy due to the predominant influence of water-column
202 optical properties on the apparent spectral characteristics of seagrass and sand bottom in the northern Gulf of Mexico.
203 For *Posidonia oceanica* mapping in the Mediterranean region, the random forests method gives more accurate results
204 than SVM approaches when compared with in-situ observations (Bakirman and Gumusay, 2020). Whereas, using a
205 high spatial resolution of WorldView-2 imagery acquired over a coastal area in Florida, the neural network classifier
206 performed better than SVM for seagrass mapping (Perez *et al.*, 2020). According to Uhrin and Townsend (2016),
207 linear spectral mixture analysis (LSMA) can be used with photo interpretation to generate spatially resolved maps
208 suitable for seagrass spatial distribution and provide improved estimates of seagrass classes. Nevertheless, Chen *et al.*
209 (2016) revealed the difficulty and limitation of LSMA for mapping the fraction of scattered and heterogeneous
210 seagrass patches that are smaller than the pixel size. At Ritchie's archipelago within the Andaman and Nicobar group
211 of Islands, Bayyana *et al.* (2020) showed that Sentinel-MSI data can detect, and map submerged benthic habitat and
212 seagrass beds present at a depth of 21 m using random forest, SVM, and K-nearest-neighbour classification algorithms.
213 Besides, linear regressions were established between the field truth measurements and several vegetation indices
214 derived from SPOT-XS, Landsat-TM, and CASI Hyperspectral airborne, to measure the density of seagrass in the
215 tropical Western Atlantic (Mumby *et al.*, 1997).

216 Since the emergence of remote sensing as a new scientific discipline in the early 1970s, vegetation indices (VI's)
217 were involved as radiometric measurements of the spatial and temporal distribution of land vegetation photo-
218 synthetically active. They use the red and near-infrared (NIR) bands, the normalized difference vegetation index
219 (NDVI) was proposed by Rouse *et al.* (1974) at the dawn of remote sensing. Since these two spectral bands are
220 generally present on Earth observation and meteorological satellites, and often containing more than 90% of the

221 information relating to vegetation canopy (Bannari et al., 1995), the NDVI had taken a privileged place in the
222 NASA/NOAA Pathfinder project (James and Kalluri, 1994). Thus, it was daily derived from NOAA-AVHRR data at
223 the Earth scale. Subsequently, it was also derived every day from MODIS and SPOT-Vegetation data to produce time-
224 series products for global vegetation assessment and monitoring at the regional and global scales. Due to this glorious
225 history and its simplicity, the NDVI has become the most widely used to assess vegetation canopy. Then, this index
226 was improved in a new version named soil adjusted vegetation index (SAVI) by Huete (1988) to minimize the artefacts
227 caused by soil background on the estimation of vegetation cover fraction by incorporating a correction factor “L”. To
228 overcome the limitations of linearity and saturation, to reduce the noise of atmospheric effects, and to remove the
229 artefacts of soil optical properties, the enhanced vegetation index (EVI) was proposed also by Huete *et al.* (2002).
230 Likewise, the transformed difference vegetation index (TDVI) was developed by Bannari *et al.* (2002) to describe the
231 vegetation cover fraction independently to the background artefacts, to reduce the saturation problem, and to enhance
232 the vegetation dynamic range linearly. These indices (NDVI, SAVI, EVI, and TDVI) were used to establish a close
233 relationship between radiometric responses and land vegetative cover densities, and they were implemented in the
234 ENVI image processing system.

235 In marine applications, several scientists for seagrass and algae discrimination and mapping tested these indices.
236 The NDVI extracted from SPOT-HRV images coupled with *in-situ* spectroradiometric data provided satisfactory
237 results for spatiotemporal change of seagrass beds in Bourgneuf-Bay in France (Barillé et al., 2009). Using
238 hyperspectral data, Dierssen et al. (2015) reported the potential of NDVI for SAV classes’ discrimination. Similarly,
239 Zoffoli et al. (2020) demonstrated the capability of NDVI derived from Sentinel-MSI data for seagrass percent cover
240 estimation and leaf biomass mapping to characterize its seasonal dynamics along the European Atlantic coast.
241 However, although VNIR bands are generally available in optical remote sensing satellites, it is well known that only
242 the visible bands can penetrate ocean water deeper than NIR which is largely absorbed by the water surface (Kirk,
243 1994). Thus, regardless of the concentrations of suspended sediments and/or organic matter, the visible wavelengths
244 are used to map the marine environment. Indeed, the blue penetrates deeper (~ 37 m) than any other wavelengths,
245 followed by green (~ 30 m), then red (~ 7 m), and NIR (Fig. 1) penetrates the least, being attenuated in the shallowest
246 depths around 2.5 m (Komatsu et al., 2020). Accordingly, blue, green, and red are the most suitable for sensing
247 seagrass and SAV (Silva et al., 2008). Thereby, when vegetation indices are applied in the marine environment
248 (Davranche et al., 2010; Zhao et al., 2013), always the red band is substituted by that of blue or green. Then, discussion
249 was initiated on WVI or aquatic vegetation indices (AVI). For instance, when the red was replaced by the green in
250 NDVI (Yang and Yang, 2009) and by the blue in SAVI (Villa et al., 2013) these versions were named, respectively,
251 the Normalized Difference Aquatic Vegetation Index (NDAVI or WNDVI) and Water Adjusted Vegetation Index
252 (WAVI). These two new versions were found more sensitive to seagrass LAI and percentage cover density, and
253 discriminated better among species of seagrass (Yang and Yang, 2009; Villa et al., 2013). To separate and map
254 vegetation features over some lake ecosystems in Italy, the NDAVI and the WAVI performed suitably (Villa et al.,
255 2014). As well, for open water features delineation, Mcfeeters (1996) replaced the difference between “NIR and red”
256 in the NDVI with that between “green and NIR”, and he baptised this new combination the Normalized Difference
257 Water Index (NDWI). In Taihu and Duck Lakes in China, NDVI and NDWI were used for wetland and SAV pattern

258 delineation and classification (Lin et al., 2010; Zhao et al., 2013). Likewise, the visible atmospherically resistant index
259 (VARI) was proposed by Gitelson et al. (2002a) to estimate the green vegetation fraction. While the triangular
260 greenness index (TGI) was developed by Hunt et al. (2013) based on the chlorophyll absorption features. The
261 capability of VARI and TGI was examined by Li (2018) who highlighted the advantage of VARI compared to TGI
262 for seagrass biomass mapping in Core Banks in North Carolina in the USA. Proposed by Richardson and Wiegand
263 (1977), the difference vegetation index (DVI) provided satisfactory results for mangrove cover and carbon stock
264 estimation in the estuary and marine environment (Candra et al., 2016). Moreover, the difference-index between the
265 blue and the green bands (DIF-BG) showed the best fits between observed and predicted SAV as reported by Mumby
266 et al. (1997).

267

268

[Figure 1]

269 3. Materials and Methods

270 Fig. 2 illustrates the followed methodology, which is based on a field survey to collect samples including seawater,
271 sediments, seagrass (*Halodule uninervis* and *Halophila stipulacea*) and algae (green and brown) from shallow marine
272 environment at different depths (0.50 to 7 m) of southeast Bahrain. To simulate the marine environment, an
273 experimental mode was established in a Goniometric-Laboratory and spectral measurements were performed using
274 an Analytical Spectral Devices (ASD) spectroradiometer over each separate and mixed species at different coverage
275 rate (0, 10, 30, 75, and 100%), as well as simulating the seabed with dark and clear colors. To assess the spectral
276 signatures variability that can be found among each separate or mixed species at varying coverage rates, all measured
277 spectra were analyzed and transformed using continuum-removed reflectance spectral (CRRS) approach (see section
278 3.4). Then, the spectra were resampled and convolved in the solar-reflective spectral bands of MSI and OLI sensors
279 using the *Canadian Modified Simulation of a Satellite Signal in the Solar Spectrum* (CAM5S) (Teillet and Santer,
280 1991) based on Herman radiative transfer code (RTC), and the relative spectral response profiles characterizing the
281 filters of each instrument in the VNIR bands. Afterward, convolved spectra were converted into several WVI
282 integrating the red, green, and blue bands. For comparison and sensor differences quantification, statistical fits were
283 conducted using linear regression analysis ($p < 0.05$) between reflectances in homologous bands and between the
284 examined homologous WVI derived from the two sensors data considering all samples, i.e., seawater, sediments,
285 seagrass, and algae species (individually and mixed at the considered coverage rates). The coefficient of determination
286 (R^2), difference values, and root mean square difference (RMSD) were calculated for reflectances and all versions of
287 investigated WVI's.

288

289

[Figure 2]

290 3.1. Study Site

291 The area under investigation in this research is the water boundary of the Kingdom of Bahrain (25° 32' and 26°00'N,
292 50° 20' and 50° 50'E) which is a group of islands located in the Arabian Gulf, east of Saudi Arabia and west of Qatar

293 (Fig. 3). The archipelago comprises 33 islands, with a total area of 8269 km², 9% of it is a land area (778.4 km²).
294 Along the southeast coast of Bahrain, the continental plateau extends for kilometers with a depth of less than one or
295 two meters. The main island of Bahrain is surrounded by shoal areas named “Fashts” where depths do not exceed 10
296 m (Bannar i and Kadhem, 2018). These areas generally support a variety of species of seagrass, algae, coral, and
297 fishes. Moreover, they play an important role in the hydrodynamic regime, which supports diverse biological
298 ecosystems. Fig. 3 also illustrates the reclamation and dredging operations that have occurred in the study area over
299 the past three decades where several coastal developmental projects are constructed, and others are in progress. These
300 anthropogenic activities strongly contribute to the degradation and even to the destruction of seagrass species and
301 associated coastal ecosystems.

302

303

[Figure 3]

304 3.2. Field sampling

305 Seagrass and algae samples were collected on 4th May 2017 from different meadows locations, which are characterized
306 by a depth range from 0.5 to 7 m in the south and southeast waters of Bahrain (Fig. 4a). Some locations were dominated
307 with *Halodule uninervis* (HU), others scattered, or dense patches were a mixture between HU and *Halophila*
308 *stipulacea* (HS). HU is the most dominant species (Fig. 4b), it occurs as dense or scattered meadows patches along
309 shoreline (Erfteimeijer and Shail, 2012). This species is like grass with narrow leaves (around 3 mm in width and 25
310 cm in length). Whereas, HS (Fig. 4c) has darker green leaves reaching 10 cm in length and it is widely present in the
311 Arabian Gulf. The brown (BA, Fig. 4d) and green (GA, Fig. 4e) algae were accessible near to shores and shallow
312 water in general. In addition to the sediments (Fig. 4f) and pure seawater samples, which were collected separately,
313 samples of each seagrass and algae species were selected and harvested in healthy and fresh conditions from several
314 stations within the study area. Then, they were stored separately in non-translucent plastic bags with seawater and
315 immediately placed in a cooler for transportation from the field to the laboratory. This was done to prevent structural
316 and leaf pigment damages due to the delay between sampling time and spectroradiometric measurements in the
317 Goniometric-Laboratory.

318

319

[Figure 4]

320 3.3. Spectroradiometric measurements

321 Spectroradiometric measurements were acquired in a dark BRDF Goniometric-Laboratory above each separated and
322 mixed samples (Fig. 5) using an ASD spectroradiometer (ASD Inc., 2015). This instrument is equipped with two
323 detectors operating in the VNIR and shortwave-infrared (SWIR), between 350 and 2500 nm. It acquires a continuous
324 spectrum with a 1.4 nm sampling interval from 350 to 1000 nm and 2 nm from 1000 to 2500 nm. The ASD resamples
325 the measurements in 1-nm intervals, which allows the acquisition of 2151 contiguous hyperspectral bands per
326 spectrum. The sensor is characterized by the programming capacity of the integration time, which allows an increase
327 of the SNR and stability. The data were acquired at nadir with a field of view (FOV) of 25° and a solar zenith angle

328 of approximately 5° by averaging 40 measurements. The ASD was installed on a BRDF Goniometric-System with a
329 height of approximately 65 cm over the target, which makes it possible to observe a surface of ~ 830 cm². A laser
330 beam was used to locate the center of the ASD-FOV. The reflectance factor of each sample was calculated by rationing
331 target radiance to the radiance obtained from a calibrated “Spectralon panel” according to the method described by
332 Jackson et al. (1980). Moreover, the corrections were applied for the wavelength dependence and non-lambertian
333 behavior of the panel (Sandmeier et al., 1998; ASD, 2015; Ben-Dor et al., 2015). The measurements were carried out
334 above each collected sample including seawater, sediments, seagrass, and algae species as well as mixed species
335 (seagrass and algae) considering different coverage rates (0, 10, 30, 75, and 100%). Each sample was placed and
336 measured twice in black and clear-bright (yellow) large bowls, considering two sedimentary substrates (dark and clear-
337 bright) underlying the seagrass and algae samples that were submerged by seawater, i.e., simulating the aquatic
338 environment. Since the remote sensing of benthic aquatic vegetation is mostly limited to the VNIR ranges (Fig. 1)
339 only the wavelengths interval between 400 and 1000 nm are considered in our analyses.

340

341

[Figure 5]

342 **3.4. Continuum-removed reflectance spectral (CRRS) transformation**

343 Spectral signatures are processed and transformed using numerous approaches to retrieve information about change
344 in absorption features (position, depth, width, and asymmetry) of a particular target over a specific bandwidth between
345 350 and 2500 nm (Van-Der-Meera, 2004). To emphasize these absorption features, many approaches were proposed
346 including relative absorption-band-depth (Crowley et al., 1989), spectral feature fitting technique, and Tricorder and
347 Tetracorder algorithms (Clark et al., 2003). These approaches work on the so-called CRRS approach, thus recognizing
348 that the absorption in a spectrum has a continuum and individual absorption features (Clark *et al.*, 1987; Van-Der-
349 Meera, 2004; Clark *et al.*, 2014). Proposed by Clark and Roush (1984), CRRS transformation and analysis allows the
350 isolation of individual absorption features in the hyperspectral signature of a specific target under investigation,
351 analysis, and comparison. It normalizes the original spectra and helps to compare individual absorption features from
352 a common baseline (Clark *et al.*, 1987). The continuum is a convex hull fit over the top of a spectrum under study
353 using straight-line segments that connect local spectra maxima. The first and last spectral data values are on the hull;
354 therefore, the first and last bands in the output continuum-removed data file are equal to 1.0. In other words, after the
355 continuum is removed, a part of the spectrum without absorption features will have a value of 1, whereas complete
356 absorption would be near to 0, and with most absorptions falling somewhere in between. The CRRS approach was
357 used for discriminating and mapping rocks mineralogy (Clark et al., 1990; Clark and Swayze, 1995), land vegetation
358 cover (Kokaly et al., 2003; Huang et al., 2004; Manevski et al., 2011), and seagrass and SAV (Barillé et al., 2011;
359 Bargain et al., 2012; Wicaksono et al., 2019; Indayani et al., 2020). In this study, the continuum algorithm
360 implemented in the ENVI image processing system was used (ENVI, 2012).

361 **3.5. Spectral sampling and convolving in MSI and OLI spectral bands**

362 Since 1972, the Landsat scientific collaboration program between NASA and USGS constitutes the continuous record
363 of the Earth's surface reflectivity from space. Indeed, the Landsat satellites series support five decades of a global
364 medium spatial resolution data collection, distribution, and archive of the Earth's surfaces (Bannari et al., 2004;
365 Loveland and Dwyer, 2012) to support research, applications, and climate change impacts analysis at the global, the
366 regional and the local scales (Roy et al., 2014 and 2016; Wulder et al., 2015). Benefiting from the acquired space-
367 engineering experience, from the heritage of Landsat instruments, and the advanced development of technology during
368 the last five decades, the fourth generation of Landsat is composed of two similar sensors with very high spectral and
369 radiometric sensitivities: OLI-1 and OLI-2 (Markham et al., 2016; Li and Chen, 2020). The OLI-1 carried onboard
370 Landsat-8 was launched on 11th February 2013, and OLI-2 onboard Landsat-9 was launched on 27th September 2021
371 (NASA, 2019 and 2021). The OLI sensors collect land-surface reflectivity in the VNIR, SWIR, and panchromatic
372 wavelength with a FOV of 15° covering a swath of 185 km with 16 days' time repetition at the equator. The band
373 passes are narrower to minimize atmospheric absorption features (NASA, 2014), especially the NIR spectral band
374 (0.865 µm). Two new spectral bands have been added: a deep blue visible shorter wavelength (band 1: 0.433 - 0.453
375 µm) designed specifically for water resources and coastal zone investigation and a new SWIR band (9: 1.360 - 1.390
376 µm) for the detection of cirrus clouds. Moreover, compared to previous TM and ETM+ sensors using only 8 bit, the
377 OLI design results in more sensitive instruments with a significant improvement of the SNR radiometric performance
378 quantized over a 12-bit dynamic range (Level 1 data), and raw data are delivered in 16 bit. The high performance of
379 SNR associated with improved radiometric and spectral resolutions provide a superior dynamic range of radiance by
380 reducing saturation problems and, therefore, enabling better characterization of land and water surface conditions
381 (Knight and Kvaran, 2014), especially with orbit reflective radiometric calibration better than 3% (Markham et al.,
382 2014; Gascon et al., 2017). Table 1 summarizes the effective bandwidth characteristics of OLI-1 and OLI-2 sensors.

383

384

[Table 1]

385

386 Otherwise, the Sentinel-2 mission is the result of close collaboration between the European Space Agency, the
387 European Commission, industry, service providers, and data users. It is composed of two satellites, Sentinel 2A and
388 2B that were launched in June 2015 and in March 2017, respectively. Both satellites are equipped with identical MSI
389 sensors to provide continuity to the SPOT missions and to improve the Landsat-OLI temporal frequency (Drusch et
390 al., 2012). The synergy between the four sensors (MSI-2A, MSI-2B, OLI-1, and OLI-2) significantly increase the
391 temporal resolution (around 2 days) offering new opportunities for several environmental and natural resource
392 applications, such as the vigour of vegetation cover, emergency management, water quality, seagrass meadows, and
393 climate change impacts analysis at local, regional, and global scales. The MSI images the Earth's surface reflectivity
394 with a large FOV (20.6°) in 13 spectral bands with several spatial resolutions from 10 to 60-m; four bands with 10-m
395 (blue, green, red, and NIR-1), six bands with 20-m (Red-Edge, NIR-2, and SWIR), and three bands with 60-m (coastal,
396 water vapor and cirrus). The swath of each scene is 290 km, permitting global coverage of the Earth's surface every
397 10 days. The MSI radiometric performance is coded in 12 bits, ensuring radiometric calibration accuracy of better

398 than 3% and an excellent SNR (Markham et al., 2014; Li et al., 2017). Table 1 summarizes the effective bandwidth
 399 characteristics of MSI-2A and MSI-2B sensors.

400 As discussed above, the measured bidirectional reflectance factors with the ASD have a 1-nm interval allowing
 401 the acquisition of 2151 contiguous hyperspectral bands per spectrum. However, most multispectral remote sensing
 402 instruments measure integrated reflectance over broad bands (equation 1). Consequently, the average of 40 spectra
 403 measured with the ASD over each sample was resampled and convolved to match the solar-reflective spectral
 404 responses functions characterizing the optics and electronics of MSI and OLI instruments in the VNIR spectral bands
 405 (Fig. 6). In this step, the resampling procedure considers the nominal width of each spectral band (Table 1). Then, the
 406 convolution process was executed using the CAM5S transfer radiative code (Teillet and Santer, 1991). This
 407 fundamental step simulates the signal received by the considered sensors at the top of the atmosphere from a surface
 408 reflecting solar and sky irradiance at sea level, considering the filter of each band (Fig. 6), and assuming ideal
 409 atmospheric conditions without scattering or absorption (Zhang and Roy, 2016). Accordingly, the equivalent
 410 convolved reflectance ($\rho(\lambda_i, \lambda_s)_i$) over each sample was generated at the satellite orbit altitude in homologous VNIR
 411 spectral bands of each sensor (Slater, 1980):

$$412 \quad \rho(\lambda_i, \lambda_s)_i = \frac{\int_{\lambda_i}^{\lambda_s} R(\lambda).S(\lambda).d(\lambda)}{\int_{\lambda_i}^{\lambda_s} S(\lambda).d(\lambda)} \quad (1)$$

414
 415 Where $\rho(\lambda_i, \lambda_s)_i$ is the equivalent convolved reflectance of the band “i” of each sensor, λ_i to λ_s are the spectral
 416 wavelength ranges of the band “i” of each sensor, $R(\lambda)$ is the corresponding reflectance at wavelength “ λ ” measured
 417 by the ASD, and $S(\lambda)_i$ is the corresponding spectral responsivity value of the spectral response function of the band
 418 “i” of each sensor (Fig. 6). It is important to note that the MSI-NIR-2 broadband (band-8: 785 - 900 nm) is not
 419 considered in this study because it is not a real homologous band of OLI-NIR, and it has a greatest reflective band
 420 difference with the OLI-NIR (851–879 nm). The OLI-NIR spectral response function intersects with only 20% of the
 421 MSI-NIR-2 response function. Moreover, the MSI red-edge bands were not considered also as they are not acquired
 422 by the OLI sensor.

423

424 [Figure 6]

425 3.6. Data Processing

426 In addition to remote sensing sensor technologies’ improvement and innovation, a variety of processing methods have
 427 been applied for spectral data for mapping and monitoring seagrass and habitats in shallow coastal waters. They were
 428 applied to highlight the seagrass and algae species composition, leaf area index estimation, percentage cover mapping,
 429 etc. They include matched filtering approach (Li et al., 2012), object-based image analysis (Roelfsema *et al.*, 2014),
 430 adaptive coherence estimator and constrained energy minimization (Li et al., 2012), artificial neural network model
 431 (Perez et al., 2020), linear spectral mixture analysis (Uhrin and Townsend, 2016; Chen et al., 2016), spectral angle
 432 mapper (Peneva et al., 2008; Li et al., 2012; Marcello et al., 2018; Wicaksono et al., 2019), classification tree analysis

433 (Wicaksono et al., 2019), random forest (Bayyana et al., 2020), support vector machines (Marcello et al., 2018;
 434 Bakirman and Gumusay, 2020; Perez et al., 2020; Bayyana et al., 2020), and machine learning regression (Traganos,
 435 2020; Bakirman and Gumusay, 2020). Undeniably, these sophisticated and complicated methods require extensive
 436 training information and field endmember measurements. However, the simplicity of empirical and semi-empirical
 437 methods based on vegetation indices are easier to transfer between sensors and can be used as a robust alternative
 438 compared to the complex processing methods; because these methods are based on the knowledge of spectral
 439 absorption features that characterize specifically the target under investigation. Moreover, these methods have the
 440 advantage of being reproducible, easily transferable, and applicable in other geographic regions. Each method has
 441 advantages and limitations, especially in shallow water. In this study, after the spectral analysis and CRRS
 442 transformation, the capability and comparison of the VNIR homologous spectral bands of MSI and OLI sensors were
 443 investigated for seawater, sediments, seagrass, algae, and mixed species discrimination at different coverage rates.
 444 Then, although the literature refers to more than fifty vegetation indices for land vegetation cover monitoring and
 445 characterization (Bannari et al., 1995), only the most popular indices that have been used for seagrass and SAV in
 446 different marine environments around the world were retained in this study. After spectral data pre-processing,
 447 sampling, and convolving, the indices TGI, VARI, and Diff(G-B) were implemented and tested respecting their
 448 original and unchangeable equations. While the NDVI, SAVI, EVI, TDVI, NDWI, and DVI indices were calculated
 449 in three versions by integrating the red, blue, and green bands. The equations of the considered indices are as follow:

$$451 \quad \text{NDVI} = (\rho_{\text{NIR}} - \rho_{\text{Red}}) / (\rho_{\text{NIR}} + \rho_{\text{Red}}) \quad (\text{Rouse et al., 1974}) \quad (2)$$

$$452 \quad \text{SAVI} = 1.5 * (\rho_{\text{NIR}} - \rho_{\text{Red}}) / (\rho_{\text{NIR}} + \rho_{\text{Red}} + 0.5) \quad (\text{Huete, 1988}) \quad (3)$$

$$453 \quad \text{TDVI} = 1.5 * (\rho_{\text{NIR}} - \rho_{\text{Red}}) / (\sqrt{(\rho_{\text{NIR}}^2 + \rho_{\text{Red}} + 0.5)}) \quad (\text{Bannari et al., 2002}) \quad (4)$$

$$454 \quad \text{NDWI} = (\rho_{\text{Green}} - \rho_{\text{NIR}}) / (\rho_{\text{Green}} + \rho_{\text{NIR}}) \quad (\text{McFeeters, 1996}) \quad (5)$$

$$455 \quad \text{EVI} = 2.5 * (\rho_{\text{NIR}} - \rho_{\text{Red}}) / (\rho_{\text{NIR}} + 6 * \rho_{\text{Red}} - 7.5 * \rho_{\text{Blue}} + 1) \quad (\text{Huete et al., 2002}) \quad (6)$$

$$456 \quad \text{DVI} = \rho_{\text{NIR}} - \rho_{\text{Red}} \quad (\text{Richardson and Wiegand, 1977}) \quad (7)$$

$$457 \quad \text{VARI} = (\rho_{\text{Green}} - \rho_{\text{Red}}) / (\rho_{\text{Green}} + \rho_{\text{Red}} - \rho_{\text{Blue}}) \quad (\text{Gitelson et al., 2002a}) \quad (8)$$

$$458 \quad \text{TGI} = \rho_{\text{Green}} - 0.39 * \rho_{\text{Red}} - 0.61 * \rho_{\text{Blue}} \quad (\text{Hunt et al., 2013}) \quad (9)$$

$$459 \quad \text{Diff(G-B)} = \rho_{\text{Blue}} - \rho_{\text{Green}} \quad (\text{Mumby et al., 1997}) \quad (10)$$

460

461 The wavelength ranges of the used VNIR bands for Sentinel-MSI and Landsat-OLI are summarize in Table 1.

462 3.7. Statistical analyses

463 As discussed previously, the MSI and OLI relative spectral response profiles characterizing the filters of each spectral
 464 band are relatively different (Fig. 6). To examine the impact of this difference, statistical analyses were computed
 465 using “Statistica” software. The relationships between the product values (reflectances and WVI’s) derived from MSI
 466 against those obtained from OLI were analyzed between homologous bands using a linear regression model ($p < 0.05$).
 467 As well, the R^2 was used to evaluate the strength of this linear relationship. For this process, the resampled and
 468 convolved spectra of all samples’ reflectance data were used, and the homologous values in VNIR bands of MSI and

469 OLI were compared using the 1:1 line. Ideally, these independent variable values should have a correspondence of
 470 1:1. Additionally, the root mean square difference (RMSD) between both sensors was derived (Willmott, 1982; Zhang
 471 et al., 2018):

$$472 \text{ RMSD} = \sqrt{\frac{\sum_i^n (v_i^{OLI} - v_i^{MSI})^2}{n}} \quad (11)$$

474
 475 Where RMSD between corresponding Landsat-OLI and Sentinel-MSI variables values (reflectances and WVI's), " v_i "
 476 is the variable under analysis and " i " is the number of variable ($i = 1$ to n).

477 4. Results analysis

478 4.1. Spectral and CRRS analysis

479 Spectral signatures of seagrass and algae species are measured separately and mixed in black and yellow large bowls
 480 using two sedimentary substrates (dark and bright). They are presented separately for the examined coverage rates,
 481 namely 10, 30, 75, and 100% (Fig. 7, a-d). Overall, the reflectance signatures of seagrass and algae samples are similar
 482 to those of healthy vegetation canopy. These reflectance signatures exhibit slight absorption features near 450 nm and
 483 others stronger between 650 and 700 nm with a minimum at 670 nm caused by the chlorophyll; as well as a significant
 484 reflection between 520 and 600 nm due to carotenoid pigments and high reflectance in the NIR attributed to internal
 485 tissue structure (700 to 900 nm). Differently to land vegetation, the red-edge is not well developed (very weak)
 486 particularly for non-dense seagrass and algae due to high red and NIR absorption by water molecules as shown in Fig.
 487 1. Generally, absorption or reflection of pigmentations between species occurs in different wavelengths but the
 488 strength of absorption gradually increases in the red as the coverage rate increases.

489 For scattered and low coverage ($\sim 10\%$), the shapes of all spectra are relatively similar, without the possibility to
 490 identify specific absorption features or to separate among species according to their spectra in the visible domain (Fig.
 491 7a). The highest reflectance values vary between 10% and 15% across NIR wavelengths with a difference reflectance
 492 ($\Delta\rho_{\text{NIR}}$) around 5%, while in the visible all the reflectance values are below 5% with $\Delta\rho_{\text{visible}}$ are also $< 5\%$. For this
 493 low and sparse cover, it is observed that the reflectance is influenced by spectral properties of the underlying
 494 sediments, fragments of vegetation, light shading, etc., thus contributing to the confusion between spectral signatures.
 495 Definitely, under such conditions, it is a challenge to distinguish between seagrass and/or algae species based only on
 496 their spectral signatures. Whereas, the measurements acquired over somewhat denser coverage rates ($\sim 30\%$) show
 497 analogous spectral behaviour and patterns with overlap among spectra in visible wavelengths (400 to 700 nm), but a
 498 slight separability between species stands out relatively in NIR (Fig. 7b).

499 Furthermore, unlike scattered or less dense cover ($\leq 30\%$), the analysis of the dense and very dense coverage rates
 500 (75 and 100%) showed that the optical properties (darkness or brightness) of the underlying substrate does not have a
 501 significant effect on the measured spectra. For these coverage ranges, the clear and normal behaviour of vegetation
 502 cover spectra are observed. The absorption feature is weak in the blue (450-480 nm) but more accentuated in red (670

503 nm), the reflection peak is more highlighted in green (550 nm), and the reflectance values increase notably and
504 gradually in NIR with the increase of the coverage rate. Although the seagrass has a distinct spectral response
505 compared to the algae, especially in the green and NIR regions of the spectrum, significant spectral differences are
506 noted for the HU with the highest reflectance, followed by GA, HS, and BA. This order is probably controlled by the
507 leaves structures that are specific for each type of seagrass or algae. The reflectance values in the visible are controlled
508 by the absorption of chlorophyll pigmentations in blue and red wavelengths, and by the carotenoid pigmentations in
509 the green band. In addition, compared to HS and BA spectra, HU and GA showed relatively strong absorption by
510 chlorophyll in red wavelengths. This difference is due to the nature of chlorophyll in each species. Indeed, brown
511 algae contain accessory pigments “fucoxanthin” and chlorophyll “c” (Johnsen and Sakshaug, 2007), while seagrass
512 are flowering plants, and their leaves contain chlorophyll “b” (Cummings and Zimmerman, 2003). It is observed also
513 that the BA carotenoid pigments (fucoxanthin) are characterized by spectral features at 630 and 650 nm that are not
514 present in the spectra of HS, HU, and GA (Fig. 7). However, despite all these spectral characteristics the difference in
515 reflectance values among all species (individual and mixed) is $\leq 6\%$ in the visible and $\leq 13\%$ in NIR for a very dense
516 cover (100%). Therefore, these results suggest that it is probably possible for the blue, green, and NIR wavelengths
517 to discriminate among the considered seagrass and algae species if they are homogeneous with high or very high
518 densities.

519 Otherwise, the CRRS transformations are presented in Fig. 7 (e-h) with Sentinel-MSI relative spectral response
520 profiles characterizing the filters of VNIR bands. The lower CRRS values indicate the greatest potential spectral
521 separability, which means the identification of the appropriate wavelengths to discriminate among the considered
522 classes of investigated species. As shown in Fig. 7 (e-h), the CRRS significantly enhances the spectral separability
523 among the seagrass and algae classes, especially in the visible bands. Two main absorption features are highlighted in
524 the blue (485-498 nm) and red (~ 670 nm) regardless the species. In the green, one major reflection peak is observed
525 around 544 nm for HU and GA, one around 530 nm for HS, and three peaks are well distinguished for BA at 578,
526 595, and 640 nm (Fig. 7h). These differentiation features become clearer as the coverage rates increase especially in
527 blue and NIR wavelengths. For a low coverage rate ($\sim 10\%$), the strongest absorption depth is that of GA (0.46)
528 followed by HU (0.58), HS (0.74), and BA (0.78) in the blue (Fig. 7e). While in the red, CRRS pointed out that
529 regardless of the coverage rate, a strong similarity is observed between HU and GA due to their high content of
530 chlorophyll pigmentation with a depth of absorption around 0.29. Subsequently followed by HS and BA that are
531 characterized by less absorption depth (~ 0.50). In these two waveband domains (blue and red), the absorption features
532 become deeper with increasing coverage density. Likewise, when the cover rate of all species becomes denser (100%),
533 similar absorption characteristics are exhibited in the red band between HU and GA species; as well as between HS
534 and BA (Fig. 7h). While in the blue and NIR wavelengths, the CRRS highlights the distinction and differentiation
535 between species. On the other hand, as the coverage increases from 10 to 100%, the reflection peak in the green
536 waveband becomes less pronounced due to the high content of carotenoid pigment; also a strong similarity is observed
537 between HU and GA. Moreover, the curves of CRRS of the mixed species occupy an intermediate position of
538 absorption features between the homogeneous samples and, therefore, the differentiation between absorption
539 characteristics becomes very narrow. Accordingly, the discrimination between pure and mixed species becomes very

540 difficult or even impossible. Overall, spectral and CRRS analyses highlighted the importance of the blue, green, and
541 NIR wavelengths for seagrass and algae detection and probable discrimination based on hyperspectral measurements.
542 These results corroborate the physical concept presented in Fig. 1 that the blue and green electromagnetic radiation
543 penetrates a deeper vertical column of water. While despite its limited penetration, the NIR shows a certain sensitivity
544 to the biomass density and its spatial distribution.

545

546 [Figure 7]

547 4.2. Resampling and convolving in OLI and MSI bands

548 Fig. 8 illustrates the scatter-plots between the resampled and convolved reflectance values in the VNIR homologous
549 bands of the MSI and OLI sensors. Simulated at the top of the atmosphere using all considered samples (seawater,
550 sediments, seagrass, algae and mixed species of both seagrass and algae at unlike coverage rates), they allow the
551 analysis of the difference in reflectance values ($\Delta\rho$) and RMSD due exclusively to dissimilarities in spectral response
552 function between homologous bands. These scatter-plots reveal a near-perfect fit with 1:1 line expressing an excellent
553 coefficient of determination (R^2 of 0.999) between homologous bands with the slopes and intercepts very near to unity
554 and zero, respectively. Thus, the derived $\Delta\rho$ values are null for VNIR homologous bands for seawater and are
555 insignificant for dark and bright substrate sediments in all bands (i.e., 0.009 for green and 0.002 for the coastal, blue,
556 red, and NIR bands). While, for seagrass and algae (HS, HU, GA, and BA), $\Delta\rho$ vary between 0.003 and 0.02 regardless
557 of the coverage rate or the considered spectral band. Moreover, the achieved overall RMSD in reflectance between
558 MSI and OLI homologous bands considering all samples are insignificant (≤ 0.0015) for blue, green, and red bands,
559 and null for coastal and NIR bands. It is also observed that all the bands are insensitive to the variation of the colors
560 of the bowls and the sedimentary substrate optical properties. These results pointed out that MSI and OLI sensors are
561 spectrally similar and can be used jointly for high temporal frequency to monitor seagrass and algae dynamics in time
562 and space. Therefore, due to this near-perfect spectral similarity between these instruments, our analysis in the
563 following sections will focus only on the MSI sensor.

564

565 [Figure 8]

566

567 Fig. 9 illustrates the reflectances of seagrass, algae, and seawater resampled and convolved in VNIR bands of MSI or
568 OLI sensors considering each species separately and all species at different coverage rates. Compared to the measured
569 hyperspectral signatures (Fig. 7), these broadband spectra are more generalized and less precise because these spectra
570 lost the specific and unique absorption features of seagrass and/or algae species caused by pigmentations as discussed
571 above. However, such broadband spectra retain the same spectral pattern as the original spectra. Regardless of the
572 species, the graphics summarized in Fig. 9 exhibit similar shape and pattern, but with a slight difference in reflectance
573 values between species in the visible bands. If we consider the species separately (HS, HU, GA, and BA) in different
574 coverage rates (10, 25, 75, and 100%), the reflectance difference values ($\Delta\rho$) are ≤ 0.02 ; and insignificant ($\Delta\rho \leq 0.002$)
575 for pure seawater and sediments in all VNIR bands. Hence, these species are not spectrally distinguishable particularly

576 in the visible whatever the coverage. While, if we consider all samples (seagrass, algae, and mixed) in all coverage
577 rates (Fig. 9e), the $\Delta\rho$ are equal to 0.03 in coastal and blue bands, 0.05 in green, 0.035 in red and 0.21 in NIR. Except
578 for the NIR, the calculated $\Delta\rho$ values in the visible are approximately identical to the accuracies achieved from
579 radiometric calibration and atmospheric corrections. Therefore, relying on the multispectral bandwidth of OLI and
580 MSI sensors, it is difficult or even impossible to differentiate or to map seagrass and algae individually at the species
581 level. Accordingly, SAV classes' discrimination and mapping will be discussed.

582

583

[Figure 9]

584 4.3. Vegetation indices analysis

585 In this third part, the NDVI, SAVI, EVI, TDVI, NDWI, and DVI indices were implemented and analysed in three
586 versions each by integrating the red, blue, and green bands; while the indices TGI, VARI, and Diff(G-B) were
587 calculated and tested respecting their original and unchangeable equations. In total, 21 combinations of indices were
588 calculated for each sensor. The statistical analyses ($p < 0.05$) focus on the similarity or dissimilarity between MSI and
589 OLI homologous indices, and their potential for seagrass and algae discrimination. Except for the TGI and VARI
590 indices, the results revealed an excellent linear relationship (R^2 of 0.999) between MSI and OLI products regardless
591 of the compared index and the integrated spectral bands (red, green, and blue). Overall, the scatter-plots presented in
592 Fig. 10 depict a very good fit to the 1:1 line with the slopes and intercepts very near to unity and zero, respectively.
593 However, despite its near-perfect linearity and insignificant RMSD between MSI and OLI values (0.001), the TGI
594 show a very weak and limited spatial variability with a range between 0.0 for pure seawater and 0.05 for a very dense
595 coverage (100%) of seagrass or algae (Fig. 10e). This range cannot allow the differentiation among the marine
596 environment classes, because this index was not developed for biomass sensing but was designed for crop nitrogen
597 requirements detection. Likewise, although the scatter-plot of VARI shows an excellent coefficient of determination
598 (R^2 of 0.99), this index overestimates the predicted values by MSI sensor compared to those estimated by OLI,
599 resulting in the data not fitting the 1:1 line very well (Fig. 10f). Moreover, the difference values of VARI derived from
600 MSI and OLI data vary between 0.0 and 0.14 depending on the sample species and its coverage rate, with an overall
601 RMSD of 0.03. This result can be explained by the fact that the VARI uses only the visible ranges of the spectrum
602 and does not consider the NIR band, which is the most informative about the biomass density. In addition, it was
603 developed particularly for very dense (100%) wheat crops; moreover, it was designed principally for coarse data
604 acquired by the SeaWiFS, MODIS, MISR, and MERIS sensors. According to Gitelson et al. (2002b), many factors
605 potentially decrease the accuracy of the VARI such as vegetation cover species, canopy architecture, and sun
606 illumination geometry. For wheat and corn species, this index yielded RMSE of around 10% (Gitelson et al., 2002a).
607 Therefore, the weaknesses raised for these two indices (TGI and VARI) are not caused by the impact due exclusively
608 to the dissimilarities in spectral response function between homologous bands of MSI and OLI sensors, but due to
609 their mathematical concepts that are intended for a single and specific application.

610 Furthermore, the scatter-plots presented in Fig. 10 (a-d) are showing examples of certain indices including NDWI,
611 WAVI, WEVI, and WTDVI. Overall, the indices are fitting very well the 1:1 line with R^2 of 0.99, slopes very near to

612 unity and intercepts to zero. The indices show that the derived WVI from MSI and OLI data are predicting similarly
 613 seagrass and algae species in a shallow marine environment. Considering all investigated samples in this study, the
 614 interval difference values between homologous indices vary between 0.0 and 0.01 for all versions of WTDVI, WAVI,
 615 WDWI, and Diff(G-B); while they vary between 0.0 and 0.04 for NDWI, WEVI and NDWI. These differences values
 616 are satisfactory and remain equal or less than the combined inaccuracies of atmospheric corrections and sensor
 617 radiometric calibration. Moreover, the achieved RMSD values between MSI and OLI homologous indices are
 618 insignificant ($RMSD \leq 0.01$) for all indices (Table 2) regardless of the integrated spectral band. These analyses pointed
 619 out that MSI and OLI sensors can be combined for high temporal frequency to monitor the dynamic of biophysical
 620 products in time and space in a shallow marine environment.

621

622 [Table 2]

623

624 [Figure 10]

625

626 Fig. 11 summarises the linear regressions ($p < 0.05$) between the best indices and the reflectances in NIR considering
 627 all samples, i.e., seawater, sediments, seagrass, algae, and mixed species classes with different coverage rates (10, 30,
 628 75, and 100%). The computed indices (NDVI, SAVI, EVI, TDVI, NDWI, and DVI) with the blue, green, and red
 629 bands are the most relevant for SAV differentiation and mapping. Firstly, it is observed that the indices NDVI and
 630 NDWI provided similar results with opposite signs, i.e., symmetrically opposed concerning the X-axis. Indeed,
 631 whatever the integrated band, the NDWI results are always symmetrical compared to those of NDVI but with negative
 632 values. However, such results are not showing the truth because negative values are automatically reset to zero by the
 633 image processing system and, therefore, it is probable that the results will be inaccurate. Furthermore, when the red
 634 and blue bands are implemented in the NDVI equation, insignificant fits (R^2 of 0.40) were achieved; but improved
 635 results are obtained with the integration of the green band (R^2 of 0.63) and the index is named NDWVI. Analogous
 636 results are obtained by Diff(G-B) and VARI indices with R^2 of 0.63 (Table 2) when all samples are considered.
 637 Luckily, the statistical fits of these three indices (NDWVI, Diff(G-B), and VARI) becomes significantly improved
 638 when unique species is considered, such as only seagrass or only algae (R^2 of 0.85). Whereas, in addition to its
 639 weakness and limited sensitivity to the spatial variability of seagrass and algae, the TGI was irrelevant for SAV
 640 discrimination yielding a very low fits (R^2 of 0.20) whatever the considered species.

641

642 [Figure 11]

643

644 As discussed previously, when integrating the blue and green bands, the indices WDWI, WAVI, WEVI, and
 645 WTDVI outperformed all examined indices regardless of the species (seagrass, algae, or mixed), yielding a very
 646 significant coefficient of determination for mixed species ($0.89 \leq R^2 \leq 0.96$) (Fig. 11 a-d, and Table 2). Calculated
 647 with blue, green, or red bands, the DVI (noted WDWI) discriminated among SAV classes significantly ($R^2 \leq 0.92$),
 648 but it underestimates the SAV as shown in Fig. 10-d. However, WAVI, WEVI, and WTDVI offer similar trends

649 regardless the considered species ($R^2 \leq 0.92$ for mixed or seagrass only, and R^2 of 0.82 for algae only). Overall, instead
650 of the red band, the integration of blue and green bands in vegetation indices increases their discriminating power for
651 SAV (Table 2). These results corroborate the spectral analysis and the CRRS transformations; the blue and green
652 electromagnetic radiation penetrates deeper through the water allowing more details and information about marine
653 vegetation discrimination. This finding is consistent with Wicaksono and Hafizt (2013), and Villa et al. (2014) where
654 the blue band better separates and maps aquatic vegetation features over some lake ecosystems in Italy. However, the
655 summarized R^2 in Table 2 shows that the indices WAVI, WEVI, and WTDVI provided relatively identical results
656 when integrating the blue or green bands. Nevertheless, the scatter plots in Fig. 11 (a, b, and c) illustrate that when the
657 green band is considered instead of the blue, the majority of sampled points are located closer to line 1:1, especially
658 when the coverage rate becomes denser. This can be explained by the fact that despite the power of blue wavelengths
659 to penetrate deeper into the water, this band also leads to an overestimation of indices values due to its higher scattering
660 (Fig. 11), mainly in turbid environments.

661 5. Discussion

662 Seagrass and algae species showed similar spectral signature curves, but with subtle differences between species. In
663 general, some relevant wavelengths are observed for the characterization of the considered species of seagrass and
664 algae including those at or near 450, 500, 520, 550, 600, 620, 640, 670, and 700 nm. They are related to the absorption
665 features and reflection peaks due to photosynthetic pigmentations of HU, HS, GA, and BA. Spectral and CRRS
666 analyses highlighted the importance of the blue, green, and NIR wavelengths for probable differentiation between the
667 considered seagrass and algae types. However, the magnitude of the $\Delta\rho$ values among species is an indicator of the
668 strength of the absorption feature depths and, therefore, of their discriminating power between species. For instance,
669 the highest $\Delta\rho$ values among all considered samples (seagrass, algae, and mixed of both) is $\leq 5\%$ across the visible
670 wavelengths and around 10 to 15% in NIR. Likewise, the CRRS transformations of all spectra of homogeneous and
671 mixed samples show that the absorption characteristics become all very similar and, thus, the discrimination between
672 pure and mixed species becomes difficult or even impossible. These results are in agreement with other findings that
673 have been conducted in many geographic locations worldwide and have considered many seagrass and algae types.
674 Considering nine tropical species of seagrass, Wicaksono et al. (2019) showed that even hyperspectral data will not
675 improve discrimination between seagrass and algae at the species level in pixels or sub-pixels due to the subtle
676 difference in absorption features among them. As well, Phinn *et al.* (2008) confirmed that the hyperspectral data are
677 unable to map seagrass biomass at the species level in shallow waters of Moreton Bay in Australia. Using field and
678 laboratory hyperspectral measurements over several seagrass species on the west coast of Florida, Pu et al. (2012)
679 reported also that the VNIR wavelengths have relatively low accuracies to discriminate among seagrass community
680 composition.

681 Otherwise, the resampled and convolved spectra in VNIR bands of MSI and OLI sensors are similar in all cases,
682 considering each species separately or the totality of samples at different coverage rates. These spectra are more
683 generalized and less precise due to the loss of absorption features caused by pigmentations. Hence, regardless of the

684 coverage rates, if uniform and homogenize species are considered, the $\Delta\rho$ is ≤ 0.02 in the visible and is ≤ 0.22 in NIR.
 685 While, if all mixed samples and species are considered at the investigated coverage rates, $\Delta\rho$ is ≤ 0.05 in visible bands
 686 and remains stable ($\Delta\rho \leq 0.22$) in NIR. These very small values do not allow spectral distinction among species,
 687 particularly in the visible wavebands. Therefore, based on the multispectral bandwidth of OLI and MSI sensors, it is
 688 difficult to differentiate seagrass and algae individually at the species level. Indeed, it is important to remember that
 689 these simulations were conducted in a Goniometric-Laboratory using close range measurements protocol and
 690 supervising rigorously all measured samples, i.e., homogeneous, or mixed. Moreover, in this controlled environment,
 691 the atmospheric scattering and absorption are absent; errors related to the sensor radiometric calibration are also
 692 absent, no wave's variation, no residual clouds contamination, no sun-glint (specular effects), no variability in water
 693 depth, and no BRDF impact. However, the results obtained are not entirely conclusive and do not provide a clear and
 694 satisfactory distinction among the spectral signatures of the investigated species. The difference among spectral
 695 signatures is surely reduced in the real world when seagrasses and algae are embedded in sediments and overlaid by
 696 water column and constituents including phytoplankton, suspended organic and inorganic matter, variability in water
 697 depth, and remote sensing problems (internal and external). Additionally, the acquired images with Sentinel-MSI (2A
 698 and 2B) and Landsat-OLI (8 and 9) sensors are coded radiometrically in 12 and 16 bits, respectively. These images
 699 cover dissimilar pixels surfaces of 100 m^2 for MSI and 900 m^2 for OLI, where SAV information can be easily mixed
 700 within pixels. Besides, the FOV of these instruments are different, OLI's FOV is 15° covering a swath of 185 km,
 701 while the MSI is characterized by a large FOV of 20.6° covering a swath of 290 km, which requires the adjustments
 702 to reduce differences caused by BRDF effects (acquisition and sun illumination geometries). Data quality may also
 703 change due to the sensor's radiometric performance, SNR, and atmospheric interferences (diffusion and absorption).
 704 Nevertheless, despite the corrections of all these anomalies before the information extraction, biases still occur
 705 generated by errors propagation, which affect the recorded signal at the sensor level and, therefore, the precision of
 706 discrimination between seagrass and algae at the species level. For instance, if we consider the published RMSE
 707 regarding each source of error separately, the calculated total RMSE based on errors propagation theory (equation 12)
 708 will be approximately 0.08 to 0.10 (reflectance unit). Therefore, this total RMSE is greater than the achieved difference
 709 between reflectance values ($\Delta\rho \leq 0.05$), especially in the visible bands. Accordingly, it is impossible to differentiate
 710 between seagrass and algae at the species level. Likewise, this total RMSE is solely due to the limitations of remote
 711 sensing methods, but it can also be amplified by environmental restrictions of seagrass habitat, as discussed above and
 712 reported by Wicaksono and Hafizt (2013).

$$713 \quad 714 \quad \text{RMSE-Total} = [(\sigma_{\text{Sensor-drift}})^2 + (\sigma_{\text{Atmosphere}})^2 + (\sigma_{\text{Sun-glint}})^2 + (\sigma_{\text{BRDF}})^2 + (\sigma_{\text{Water-column}})^2]^{0.5} \quad (12)$$

715
 716 Where:

717 $\sigma_{\text{Sensor-drift}}$: Sensor radiometric calibration accuracy, ± 0.03 (Markhman et al., 2014 and 2016),

718 $\sigma_{\text{Atmosphere}}$: Atmospheric corrections accuracy, mostly around ± 0.03 to ± 0.05 in the visible bands (Vermote et al.,
 719 2016),

720 $\sigma_{\text{Sun-glint}}$: Sun glint correction accuracy, ± 0.05 (Zorrilla et al., 2019),

721 $\sigma_{\text{-BRDF}}$: Accuracy of BRDF correction for MSI, ± 0.05 to ± 0.08 (Roy et al., 2017),

722 $\sigma_{\text{-Water-column}}$: Accuracy of water column correction, ± 0.04 (Zoffoli et al., 2014).

723
724 The results of this research accomplished in the Arabian Gulf species based on spectroradiometric measurements are
725 consistent with other researches carried out in many geographical regions worldwide. Barillé et al. (2009) showed the
726 degradation of spectral features when resampled into SPOT-HRV visible bands and, therefore, seagrass species could
727 no longer be discriminated in these wavelengths. This statement is also in agreement with Wicaksono et al. (2017)
728 who reported that resampled spectra in MSI and OLI bands do not have sufficient spectral information for seagrass
729 species discrimination for accurate classification. Using MSI and OLI data with respectively 10 m and 30 m pixel
730 sizes (i.e., each OLI pixel is represented by 9 MSI pixels), Lyons et al. (2011) reported relatively accurate
731 discrimination between seagrass meadows spots that are very large with homogenous composition and distinct
732 boundaries between species. While, the differentiation becomes impossible when the analyzed spots are composed of
733 diverse species and scattered without clear boundary.

734 Furthermore, to analyze the impact of differences in reflectance exclusively due to dissimilarities in spectral
735 response function between homologous spectral bands, the scatter-plots between SMI and OLI simulated surface
736 reflectance values at the top of the atmosphere revealed a very good linear relationship (R^2 of 0.999) between VNIR
737 homologous bands. The slopes and intercepts are nearly equal to unity and zero, respectively. It is also observed that
738 independently to the sediments substrate (dark and bright) or the color of used bowls (black or yellow), the $\Delta\rho$ values
739 between VNIR homologous bands vary in the range of 0.003 to 0.02, regardless of the observed species (seagrass,
740 algae and mixed) or the coverage rate. Moreover, the achieved overall RMSD in reflectance values are very small (\leq
741 0.0015) for all VNIR bands, i.e., smaller than the uncertainty of the radiometric calibration process (0.03) as
742 demonstrated by Markham et al. (2016). In other respect, all the derived homologous WVI values fit near-perfectly
743 with the 1:1 line expressing an excellent coefficient of determination (R^2 of 0.99), a slope of 0.99 and intercept equal
744 to zero. Moreover, the achieved RMSD values between MSI and OLI homologous indices are insignificant ($\text{RMSD} \leq$
745 0.01) for all indices regardless of the integrated spectral band (red, green, and blue). These results corroborate the
746 finding of Wicaksono et al. (2019) who reported that MSI and OLI had similar results for tropical seagrass species
747 analysis using simulated reflectance spectra and imagery data. Moreover, using simulated data and images acquired
748 simultaneously with MSI and OLI over a wide variety of land cover types including open shallow water, Mandanici
749 and Bitelli (2016) showed a very high coefficient of determination (R^2 of 0.98) between homologous bands. Therefore,
750 these results pointed out that the examined sensors, MSI onboard Sentinel-2A/2B and OLI onboard Landsat-8/9, can
751 be combined for the marine environment and SAV detection, mapping, and monitoring during shorter time intervals
752 or for consecutive observations. However, rigorous pre-processing issues (sensors calibration, atmospheric
753 corrections, sun-glint corrections, and BRDF normalization) must be addressed before the joint use of acquired data
754 with these sensors. Furthermore, we demonstrated that blue and green bands are better than red for seagrass and algae
755 biomass discrimination, providing the best R^2 and the most insignificant RMSD for the investigated indices. Green
756 rather than the blue band integration is preferable due to its better sensitivity to pigment content within seagrass and
757 algae tissues, for its ability to penetrate water, and for its low sensibility to atmosphere and water column scattering.

758 6. Conclusions

759 The MSI sensors onboard Sentinel satellites 2A/2B and the OLI instruments installed on Landsat 8/9 satellites are
760 designed to be similar in the perspective that their data be used together to support global Earth surface reflectances
761 coverage for science and development applications at medium spatial resolution and near-daily temporal resolution.
762 However, relative spectral response profiles characterizing the filter's responsivities of these instruments are not
763 identical between the homologous bands, so some differences are probably expected in the recorded shallow water
764 reflectance values for seagrass, algae, and mixed species differentiation and mapping. Based on spectral analysis and
765 CRRS transformation, the results of the present research pointed out subtle spectral differences between seagrass (HU
766 and HS), algae (green and brown), or mixed species, particularly in the blue, green, and NIR wavelengths. However,
767 once resampled and convolved in MSI and OLI homologous VNIR bands, similar patterns to the original spectra are
768 observed but with severe generalisation and loss of specific absorption features. Therefore, mapping seagrass and/or
769 algae at the species level in shallow marine waters is a very difficult if not impossible task, either using multispectral
770 bandwidth of MSI and OLI sensors or even hyperspectral data. Moreover, different from these ideal simulations in a
771 controlled environment, the mapping would be more difficult in a real marine habitat where various species are mixed
772 and interleaved with each other, as well as the propagation of internal and external errors related to remote sensing
773 data. Hence, it is recommended to discuss SAV rather than the mapping seagrass or algae at the species level.

774 Furthermore, instead of the red band, the integration of the blue and green bands in WVI increases their
775 discriminating power and ability of map SAV, particularly WAVI, WEVI, and WTDVI indices. These results
776 corroborate the spectral analysis and the CRRS transformations that the blue and green electromagnetic radiation
777 allows better marine vegetation differentiation. Nevertheless, despite the power of blue wavelength to penetrate deeper
778 into the water, it also leads to a relative overestimation of dense SAV coverage due to the higher scattering in this part
779 of the spectrum, particularly in the turbid environment. Furthermore, statistical fits between SMI and OLI simulated
780 surface reflectance over the considered samples reveal an excellent linear relationship (R^2 of 0.999) between all
781 homologous VNIR bands. The achieved RMSD values are extremely small between the NIR homologous bands and
782 insignificant for the other bands (≤ 0.0015). Moreover, independently of the analysed samples, homogeneous (seagrass
783 or algae) or mixed (seagrass plus algae), good agreements ($0.63 \leq R^2 \leq 0.96$) were also obtained between homologous
784 WVI regardless of the integrated spectral bands (i.e., red, green, and blue), yielding insignificant RMSD (≤ 0.01).
785 These achieved RMSD values for reflectances or WVI's are less than the combined errors related to sensor radiometric
786 calibration and atmospheric corrections. Accordingly, these results pointed out that MSI and OLI sensors are spectrally
787 similar and can be combined for high temporal frequency to monitor accurately the SAV and its dynamic in time and
788 space in the shallow marine environment. However, rigorous pre-processing issues such as sensors calibration,
789 atmospheric corrections, BRDF normalisation, sun glint, and water column corrections must be addressed before the
790 joint use of acquired data with these sensors.

791
792 **7. Author Contributions:** Professor A. Bannari performed the paper conceptualization, field data collection, pre-
793 processing and processing, results analyses and paper writing. Professor S.T. Ali assisted in the field sampling, the

794 results analyses and the paper writing. Professor A. Abuhussain assisted in the results interpretation, analyses and
795 paper writing. All authors have read and agreed to the published version of the manuscript.

796

797 **8. Competing Interests:** The authors declare no conflict of interest.

798

799 **9. Acknowledgements**

800 The authors would like to thank the Arabian Gulf University (Kingdom of Bahrain) for the financial support for the
801 field data collection, and to Marine and Environment Arabia Consultancy Services (Manama, Bahrain), for providing
802 photographs and making them available for consultation and public use. Our gratitude goes also to the anonymous
803 reviewers for their constructive comments.

804

805 **10. References**

806 Anders, K. and Lina, N.: Remote sensing of seagrasses in a patchy multi-species environment. *International Journal*
807 *of Remote Sensing*, 32(8), 2227 – 2244, 2011.

808 ASD: Analytical Spectral Devices. Technical Guide, 4th ed.; ASD Inc.: Boulder, CO, USA. Available online:
809 <http://www.asdi.com/products-spectroradiometers.asp> (accessed on 30 September 2020), 2015.

810 Bakirman, T. and Gumusay, M. U.: Assessment of Machine Learning Methods for Seagrass Classification in the
811 Mediterranean. *Baltic J. Modern Computing*, 8(2), 315-326. <https://doi.org/10.22364/bjmc.2020.8.2.07> , 2020.

812 Bannari, A.: Synergy between Sentinel-MSI and Landsat-OLI to Support High Temporal Frequency for Soil Salinity
813 Monitoring in an Arid Landscape. In: *Research Developments in Saline Agriculture*, edited by Jagdish Chander
814 Dagar, Rajender Kumar Yadav, and Parbodh Chander Sharma. Published by Springer Nature Singapore Pte Ltd.,
815 pp. 67-93, ISBN: 978-981-13-5831-9. https://doi.org/10.1007/978-981-13-5832-6_3, 2019.

816 Bannari, A., Morin, D., Huete, A. R. and Bonn, F.: A Review of Vegetation indices. *Remote Sensing Reviews*, 13,
817 95-120, 1995.

818 Bannari, A., Asalhi, H. and Teillet, P. M.: Transformed Difference Vegetation Index (TDVI) for Vegetation cover
819 Mapping. *International Geoscience and Remote Sensing Symposium (IGARSS'2002)*, Toronto, Ontario, 9-13
820 July, pp. 3053-3055, 2002.

821 Bannari, A., Teillet, P. M., and Landry, R.: Comparaison des réflectances des surfaces naturelles dans les bandes
822 spectrales homologues des capteurs TM de Landsat-5 et TME+ de Landsat-7. *Revue Télédétection*, 4(3), 263-275,
823 2004.

824 Bannari, A. and Kadhem, G.: MBES-CARIS Data Validation for Bathymetric Mapping of Shallow Water in the
825 Kingdom of Bahrain on the Arabian Gulf. *Remote Sensing*, 9, 385-404, 2017.

826 Bannari, A. and Al-Ali, Z.: Ground Reflectance Factor Retrieval from Landsat (MSS, TM, ETM+, and OLI) Time
827 Series Data based on Semi-empirical Line Approach and Pseudo-invariant Targets in Arid Landscape.
828 *International Geoscience and Remote Sensing Symposium (IGARSS-2020)*, July 19-24th, Waikoloa, Hawaii,
829 USA, pp. 5990-5993, 2020.

- 830 Barillé, L., Mouget, J. L., Méléder, V., Rosa, P., Jesus, B.: Spectral response of benthic diatoms with different
831 sediment backgrounds. *Remote Sensing of Environment*, 115(4), 1034–1042, 2011.
- 832 Barillé, L., Robin, M., Harin, N., Bargain, A. and Launeau, P.: Increase in seagrass distribution at Bourgneuf Bay
833 (France) detected by spatial remote sensing. *Aquatic Botany*, 92(3), 185-194, 2010.
- 834 Bargain, A., Robin, M., Le-Men, E., Huete, A. R. and Barillé, L.: Spectral response of the seagrass *Zostera noltii* with
835 different sediment backgrounds. *Aquatic Botany*, 98, 45-56, 2012.
- 836 Bayyana, S., Pawar, S., Gole, S., Dudhat, S., Pande, A., Mitra, D., Johnson, J. A. and Sivakumar, K.: Detection and
837 mapping of seagrass meadows at Ritchie’s archipelago using Sentinel 2A satellite imagery. *Current Science*,
838 118(8), 1275-1282. DOI: 10.18520/cs/v118/i8/1275-1282, 2020.
- 839 Ben-Dor, E., Ong, C. and Lau, I. C.: Reflectance measurements of soils in the laboratory: Standards and protocols.
840 *Geoderma*, 245–246, 112–124, 2015.
- 841 Boström, C., Pittman, S., Kneib, R. and Simenstad, C.: Seascape ecology of coastal biogenic habitats: advances, gaps
842 and challenges. *Marine Ecology Progress Series*, 427, 191– 217, 2011.
- 843 Burfeind, D. D. and Stunz, G. W.: The effects of boat propeller scarring intensity on nekton abundance in subtropical
844 seagrass meadows. *Marine Biology (Berlin)*, 148, 953–962, 2006.
- 845 Candra, E. D., Hartono, and Wicaksono, P.: Above Ground Carbon Stock Estimates of Mangrove Forest Using
846 Worldview-2 Imagery in Teluk Bena, Bali. *IOP Conference Series: Earth and Environmental Science*, 47(1).
847 <https://doi.org/10.1088/1755-1315/47/1/012014>, 2016.
- 848 Chen, C.-F., Lau, A.-K., Chang, N.-B., Son, N.-T., Tong, P.-H.-S and Chiang, S.-H.: Multi-temporal change detection
849 of seagrass beds using integrated Landsat TM/ETM+/OLI imageries in Cam Ranh Bay, Vietnam. *Ecological*
850 *Informatics*, 35, 43-54, 2016.
- 851 Clark, R. N. and Roush, T. L.: Reflectance spectroscopy: Quantitative analysis techniques for remote sensing
852 applications. *Journal of Geophysical Research*, 89, 6329–6340, 1984.
- 853 Clark, R. N., King, T. V. V. and Gorelick, N. S.: Automatic continuum analysis of reflectance spectra. In JPL
854 Proceedings of the 3rd Airborne Imaging Spectrometer Data Analysis Workshop, 138-142. Available on line:
855 <https://ntrs.nasa.gov/archive/nasa/casi.ntrs.nasa.gov/19880004388.pdf> (accessed on 18 March 2021), 1987.
- 856 Clark, R. N., Gallagher, A. J. and Swayze, G. A.: Material absorption-band depth mapping of imaging spectrometer
857 data using the complete band shape least-squares algorithm simultaneously fit to multiple spectral features from
858 multiple materials. In: Proceedings of the Third Airborne Visible/Infrared Imaging Spectrometer (AVIRIS)
859 Workshop, NASA - Jet Propulsion Laboratory Publications, No. 90-54, pp. 176–186, 1990.
- 860 Clark, R. N. and Swayze, G. A.: Mapping minerals, amorphous materials, environmental materials, vegetation, water,
861 ice and snow, and other materials. The USGS Tricorder algorithm, in Green, R.O., ed., Summaries of the fifth
862 annual NASA Jet Propulsion Laboratory airborne earth science workshop: Pasadena, NASA Jet Propulsion
863 Laboratory Publication, 95(1), 39-40, 1995.
- 864 Clark, R. N., Swayze, G. A., Carlson, R., Grundy, W. and Noll, K.: Spectroscopy from Space. *Reviews in Mineralogy*
865 *and Geochemistry*, 78(1), 399-446. DOI:10.2138/rmg.2014.78.10, 2014.

- 866 Crowley, J. K., Brickey, D. W. and Rowan, L. C.: Airborne imaging spectrometer data of the Ruby Mountains,
867 Montana: mineral discrimination using relative absorption band-depth images. *Remote Sensing of Environment*,
868 29(2), 121–134. [https://doi.org/10.1016/0034-4257\(89\)90021-7](https://doi.org/10.1016/0034-4257(89)90021-7), 1989.
- 869 Cummings, M. E. and Zimmerman, R. C.: Light harvesting and the package effect in the seagrasses *Thalassia*
870 *testudinum* Banks ex König and *Zostera marina* L.: Optical constraints on photo-acclimation. *Aquatic Botany*, 75,
871 261–274, 2003.
- 872 Dahdouh-Guebas, F., Coppejans, E. and Van-Speybroeck, D.: Remote sensing and zonation of seagrasses and algae
873 along the Kenyan coast. *Hydrobiologia*, 400, 63-73, 1999.
- 874 Dattola, L., Rende, S. F., Dominici, R., Lanera, P., Di-Mento, R., Scalise, S., Cappa, P., Oranges, T. and Aramini, G.:
875 Comparison of Sentinel-2 and Landsat-8 OLI satellite images vs. high spatial resolution images (MIVIS and
876 WorldView-2) for mapping *Posidonia oceanica* meadows. Proceedings of SPIE 10784, Remote Sensing of the
877 Ocean, Sea Ice, Coastal Waters, and Large Water Regions, 10 October 2018, Vol. 10784, 1078419-1; doi:
878 10.1117/12.2326798, 2018.
- 879 Davranche, A., Lefebvre, G. and Poulin, B.: Wetland monitoring using classification trees and SPOT-5 seasonal time
880 series. *Remote Sensing of Environment*, 114(3), 552–562, 2010.
- 881 Dean, A. and Salim, A.: Remote sensing for the sustainable development of offshore mariculture. In: *A global*
882 *assessment of offshore mariculture potential from a spatial perspective*, edited by: Kapetsky, J. M., Aguilar-
883 Manjarrez, J. and Jenness, J.: FAO Fisheries and Aquaculture Technical Paper N. 549, Rome, Italy, 181 pp, 2013.
- 884 Dekker, A. G., Hestir, E. L., Malthus, T. J. and Thankappan, M.: Continental Scale Aquatic Habitat Monitoring Using
885 Sentinel-2. ESA-ESRIN, Frascati, Italy, 23 to 27 April; 28 pp, 2012
- 886 Den-Hartog, C.: The seagrasses of the world. North-Holland Publishing Company, Amsterdam, Netherland, 275 pp.
887 <https://doi.org/10.1002/iroh.19710560139>, 1970.
- 888 Dierssen, H. M., Chlus, A. and Russell, B.: Hyperspectral discrimination of floating mats of seagrass wrack and the
889 macroalgae *Sargassum* in coastal waters of Greater Florida Bay using airborne remote sensing. *Remote Sensing*
890 *of Environment*, 167, 247-258, 2015.
- 891 Drusch, M., Del-Bello, U., Carlier, S., Colin, O., Fernandez, V., Gascon, F., Hoersch, B., Isola, C. Laberinti, P.,
892 Martimort, P., Meygret, A., Spoto, F., Sy, O., Marchese, F., Bargellini, P.: Sentinel-2: ESA's optical high-
893 resolution mission for GMES operational services. *Remote Sensing of Environment*, 120, 25–36.
894 <https://doi.org/10.1016/j.rse.2011.11.026>, 2012.
- 895 Duarte, C. M. and Gattuso, J.-P.: Seagrass meadows. In *Encyclopedia of Earth*. Edited by Cutler J. Cleveland;
896 Environmental information coalition National Council for Science and the Environment, Washington, DC, USA,
897 2008.
- 898 Duarte, C. M., Losada, I. J., Hendriks, I. E., Mazarrasa, I. and Marbà, N.: The role of coastal plant communities for
899 climate change mitigation and adaptation. *Nature Climate Change*, 3(11), 961–968.
900 <https://doi.org/10.1038/nclimate1970>, 2013.

- 901 Duffy, J. P., Pratt, L., Anderson, K., Land, P. E. and Shutler, J. D.: Spatial assessment of intertidal seagrass meadows
902 using optical imaging systems and a lightweight drone. *Estuarine, Coastal and Shelf Science*, 200, 169–180, 2018.
- 903 Dunton, K. H., and Schonberg, S. V.: Assessment of propeller scarring in seagrass beds of the south Texas coast:
904 *Journal Coastal Research*, 37, 100–110, 2002.
- 905 ENVI: Continuum Removal Tutorial. Boulder, Colorado, USA.
906 <http://www.harrisgeospatial.com/docs/ContinuumRemoval.html> , 2017.
- 907 Erfteimeijer, P. L. A. and Shuaib, D. A.: Seagrass Habitats in Arabian Gulf: Distribution, Tolerance Thresholds and
908 Threats. *Aquatic Ecosystem Health and Management*, 15(1), 73-83, 2012.
- 909 Ferguson, R. L. and Wood, L. L.: Mapping Submerged Aquatic Vegetation in North Carolina with Conventional
910 Aerial Photography. Federal Coastal Wetland Mapping Programs, National Ocean Pollution Policy Board's
911 Habitat Loss and Modification Working Group. Biological Report, 90(18), pp. 125 – 132. Also available in web:
912 <https://apps.dtic.mil/sti/pdfs/ADA322827.pdf#page=123>, 1990.
- 913 Flood, N.: Comparing Sentinel-2A and Landsat 7 and 8 Using Surface Reflectance over Australia. *Remote Sensing*,
914 9, 659, 2017. DOI: 10.3390/rs9070659, 2017.
- 915 Fourqurean, J. W., Duarte, C. M., Kennedy, H., Marbà, N., Holmer, M., Mateo, M. A., Apostolaki, E. T., Kendrick,
916 G. A., Krause-Jensen, D., McGlathery, K. D. and Serrano, O.: Seagrass ecosystems as a globally significant carbon
917 stock. *Nature Geoscience*, 5(7), 505–509, 2012.
- 918 Fyfe, S. K.: Spatial and temporal variation in spectral reflectance: Are seagrass species spectrally distinct? *Limnology*
919 and *Oceanography*, 48(1, part 2), 464–479. http://dx.doi.org/10.4319/lo.2003.48.1_part_2.0464, 2003.
- 920 Gascon, F., Bouzinac, C., Thépaut, O., Jung, M., Francesconi, B., Louis, J., Lonjou, V., Lafrance, B., Massera, S.,
921 Gaudel-Vacaresse, A., Languille, F., Alhammoud, B., Viallefont, F., Pflug, B., Bieniarz, J., Clerc, S., Pessiot, L.,
922 Trémas, T., Cadau, E., De Bonis, R., Isola, C., Martimort, P. and Fernandez, V.: Copernicus Sentinel-2A
923 Calibration and Products Validation Status. *Remote Sensing*, 9, 584. <https://doi.org/10.3390/rs9060584>, 2017.
- 924 Gitelson, A. A., Kaufman, Y. J., Stark, R. and Rundquist, D.: Novel algorithms for remote estimation of vegetation
925 fraction. *Remote Sensing of Environment*, 80, 76–87, 2002a.
- 926 Gitelson, A. A., Stark, R., Grits, U., Rundquist, D., Kaufman, Y. J. and Derry, D.: Vegetation and soil lines in visible
927 spectral space: a concept and technique for remote estimation of vegetation fraction. *Int. Journal of Remote*
928 *Sensing*, 23(13), 2537–2562, 2002b.
- 929 Green, E. P. and Short, F.: World atlas of seagrasses. Prepared by the UIMEP World Conservation Monitoring Centre.
930 University of California Press, Berkeley, USA, Volume 47. Berkeley (California, USA): University of California.
931 <https://doi.org/10.1515/BOT.2004.029>, 2003.
- 932 Grech, A., Chartrand-Miller, K., Erfteimeijer, P., Fonseca, M., McKenzie, L., Rasheed, M. and Coles, R.: A
933 comparison of threats, vulnerabilities and management approaches in global seagrass bioregions. *Environmental*
934 *Research Letters*, 7(2), 024006, 2012.
- 935 Hamel, M. A. and Andréfouët, S.: Using very high resolution remote sensing for the management of coral reef
936 fisheries: review and perspectives. *Marine Pollution Bulletin*, 60(9), 1397-405. DOI:
937 10.1016/j.marpolbul.2010.07.002. Epub 2010 Jul 24, 2010.

- 938 Hashim, M., Misbari, S., Yahya, N. N., Ahmad, S., Reba, M. N. and Komatsu, T.: An approach for quantification of
939 submerged seagrass biomass in shallow turbid coastal waters. In Proceedings of IGARSS, Quebec, Canada, pp.
940 4439-4442. DOI: 10.1109/IGARSS.2014.6947476, 2014.
- 941 Hedley, J., Roelfsema, C., Koetz, B. and Phinn, S.: Capability of the Sentinel 2 mission for tropical coral reef mapping
942 and coral bleaching detection. *Remote Sensing of Environment*, 120, 145–155, 2012a.
- 943 Hedley, J. D., Roelfsema, C. M., Phinn, S. R. and Mumby, P. J.: Environmental and sensor limitations in optical
944 remote sensing of coral reefs: implications for monitoring and sensor design. *Remote Sensing*, 4, 271-302.
945 <http://dx.doi.org/10.3390/rs4010271>, 2012b.
- 946 Hossain, M. S., Bujang, J. S., Zakaria, M. H. and Hashim, M.: The application of remote sensing to seagrass
947 ecosystems: An overview and future research prospects. *Int. J. Remote Sensing*, 36(1), 61–113, 2014.
- 948 Huang, Z., Turner, B. J., Dury, S. J., Wallis, I. R. and Foley, W. J.: Estimating foliage nitrogen concentration from
949 HYMAP data using continuum removal analysis. *Remote Sensing of Environment*, 93, 18–29, 2004.
- 950 Huete, A. R.: A soil-adjusted vegetation index (SAVI). *Remote Sensing of Environment*, 25, 295-309, 1988.
- 951 Huete, A. R., Didan, K., Miura, T., Rodriguez, E. P., Gao, X. and Ferreira, L. G.: Overview of the radiometric and
952 biophysical performance of the MODIS vegetation indices. *Remote Sensing of Environment*, 83(1), 195-213.
953 [http://dx.doi.org/10.1016/S0034-4257\(02\)00096-2](http://dx.doi.org/10.1016/S0034-4257(02)00096-2), 2002.
- 954 Hunt, Jr. E. R., Doraiswamy, P. C., McMurtrey, J. E., Daughtry, C. S. T., Perry, E. M., and Akhmedov, B.: A visible
955 band index for remote sensing leaf chlorophyll content at the canopy scale. *Int. Journal of Applied Earth
956 Observation and Geoinformation*, 21, 103–112, 2013.
- 957 Indayani, A. B., Danoedoro, P., Wicaksono, P., Winarso, G. and Setiawan, K. T.: Spectral Analysis from Absorption
958 and Reflectance of Seagrass Leaves using Trios-Ramses Spectroradiometer in Nusa Lembongan and Pemuteran,
959 Bali. *Jurnal Penginderaan Jauh dan Pengolahan Data Citra Digital*, 17(2), 103-113.
960 <http://dx.doi.org/10.30536/j.pjpdcd.2020.v17.a3384>, 2020.
- 961 Irons, J. R. Dwyer, J. L. and Barsi, J. A.: The next Landsat satellite: the Landsat data continuity mission. *Remote
962 Sensing of Environment*, 122, 11–21. <https://doi.org/10.1016/j.rse.2011.08.026>, 2012.
- 963 Jackson, R. D, Pinter, P. J., Paul, J., Reginato, R. J., Robert, J. and Idso, S. B.: *Hand-Held Radiometry. Agricultural
964 Reviews and Manuals, ARM-W-19*; U.S. Department of Agriculture Science and Education Administration:
965 Phoenix, AZ, USA, 1980.
- 966 James, M. E. and Kalluri, S. N. V.: The Pathfinder AVHRR land data set: an improved coarse resolution data set for
967 terrestrial monitoring. *Int. Journal of Remote Sensing*, 15(17), 3347–3363, 1994.
- 968 Johnsen, G. and Sakshaug, E.: Biooptical characteristics of PSII and PSI in 33 species (13 pigment groups) of marine
969 phytoplankton, and the relevance for pulse amplitude-modulated and fast-repetition-rate fluorometry1. *Journal of
970 Phycology*, 43, 1236–1251, 2007.
- 971 Kibele, J.: *Submerged habitats from space: Increasing map production capacity with new methods and software. PhD
972 Thesis, Institute of Marine Science, the University of Auckland, New-Zeeland, 179 pp, 2017.*
- 973 Kirk, J. T. O.: *Light and photosynthesis in aquatic ecosystems, 2nd edition. Cambridge university press, 509 pp.*
974 <https://doi.org/10.1017/CBO9780511623370>, 1994.

- 975 Knight, E. and Kvaran, G.: Landsat-8 operational land imager design, characterization and performance. *Remote*
976 *Sensing*, 6(11), 10286–10305, 2014.
- 977 Knudby, A. and Nordlund, L.: Remote sensing of seagrasses in a patchy multi-species environment. *Int. Journal of*
978 *Remote Sensing*, 32(8), 2227–2244, 2011.
- 979 Kokaly, R. F., Despain, D. G., Clark, R. N. and Livo, K. E.: Mapping vegetation in Yellowstone National Park using
980 spectral feature analysis of AVIRIS data. *Remote Sensing of Environment*, 84, 437–456, 2003.
- 981 Komatsu, T., Hashim, M., Nurdin, N., Noiraksar, T., Prathep, A., Stankovic, M., Hoang-Son, T. P., Thu, P. M., Luong,
982 C. V., Wouthyzen, S., Phauk, S., Muslim, A. M., Yahya, N. N., Terauchi, G., Sagawa, T. and Ken-ichi
983 Hayashizaki, K.-H.: Practical mapping methods of seagrass beds by satellite remote sensing and ground trothing.
984 *Coastal Marine Science*, 43(1), 1–25, 2020.
- 985 Konstantinos, T., Spyridon, C. S., Apostolos, P. and Nikolaos, S.: The use of Sentinel-2 imagery for seagrass mapping:
986 Kalloni Gulf (Lesvos Island, Greece) case study. *Proceedings of the SPIE, Volume 9688, Fourth International*
987 *Conference on Remote Sensing and Geoinformation of the Environment (RSCy2016)*, 96881F.
988 [Doi:10.1117/12.2242887](https://doi.org/10.1117/12.2242887), <http://dx.doi.org/10.1117/12.2242887>, 2016.
- 989 Kovacs, E., Roelfsema, C., Lyons, M., Zhao, S. and Phinn, S.: Seagrass habitat mapping: how do Landsat 8 OLI,
990 Sentinel-2, ZY-3A, and Worldview-3 perform? *Remote Sensing Letters*, 9(7), 686–695, 2018.
- 991 Larkum, A. W. D., Orth, R. J. and Duarte, C. M.: Seagrasses: Biology, ecology and conservation. *Seagrasses: Biology,*
992 *Ecology and Conservation*. <https://doi.org/10.1007/978-1-4020-2983-7>, 2006.
- 993 Leleu, K., Alban, F., Pelletier, D., Charbonnel, E., Letourneur, Y. and Boudouresque, C.F.: Fishers' perceptions as
994 indicators of the performance of Marine Protected Areas (MPAs). *Marine Policy*, 36(2), 414-422.
995 <https://doi.org/10.1016/j.marpol.2011.06.002>, 2012.
- 996 Li, J. and Chen, B.: Global Revisit Interval Analysis of Landsat-8 -9 and Sentinel-2A-2B Data for Terrestrial
997 Monitoring. *Sensors*, 20, 6631. <https://doi.org/10.3390/s20226631>, 2020.
- 998 Li, J. and Roy, D. P.: A Global Analysis of Sentinel-2A, Sentinel-2B and Landsat-8 Data Revisit Intervals and
999 Implications for Terrestrial Monitoring. *Remote Sensing*, 9, 902. DOI: 10.3390/rs9090902, 2017.
- 1000 Li, S., Ganguly, S., Dungan, J. L., Wang, W. L. and Nemani, R. R.: Sentinel-2 MSI Radiometric Characterization and
1001 Cross-Calibration with Landsat-8 OLI. *Advances in Remote Sensing*, 6, 147-159. DOI : 10.4236/ars.2017.62011.,
1002 2017.
- 1003 Li, R., Liu, J.-K., Sukcharoenpong, A., Yuan, J., Zhu, H. and Zhang, S.: A Systematic Approach toward Detection of
1004 Seagrass Patches from Hyperspectral Imagery, *Marine Geodesy*, 35(3), 271-286, 2012.
- 1005 Li, S.: *Seagrass Mapping and Human Impact Evaluation Using Remote Sensing Imagery at Core Banks, North*
1006 *Carolina*. Duke University, 2018.
- 1007 Lin, C., Gong, Z. and Zhao, W.: The extraction of wetland hydrophytes types based on medium resolution TM data.
1008 *Shengtai Xuebao/Acta Ecologica Sinica*, 30(23), 6460–6469, 2010.

- 1009 Loveland, T. R. and Dwyer, J. L.: Landsat: Building a strong future. *Remote Sensing of Environment*, 122, 22–29.
1010 <https://doi.org/10.1016/j.rse.2011.09.022>, 2012.
- 1011 Lyimo, L. D.: Carbon sequestration processes in tropical seagrass beds. PhD Thesis, Department of Ecology,
1012 Environment and Plant Sciences, Stockholm University, Sweden, 2016.
- 1013 Lyons M. B., Phinn S. R. and Roelfsema C. M.: Integrating Quickbird Multi-Spectral Satellite and Field Data:
1014 Mapping Bathymetry, Seagrass Cover, Seagrass Species and Change in Moreton Bay, Australia in 2004 and 2007.
1015 *Remote Sensing*, 3, 42-64. doi:<http://dx.doi.org/10.3390/rs3010042>., 2011.
- 1016 Lyons, M. B., Phinn, S. R. and Roelfsema, C. M.: Long term land cover and seagrass mapping using Landsat and
1017 object-based image analysis from 1972 to 2010 in the coastal environment of South East Queensland, Australia.
1018 *ISPRS Journal of Photogrammetry and Remote Sensing*, 71, 34–46, 2012.
- 1019 Lyons, M. B., Roelfsema, C. M., and Phinn, S. R.: Towards understanding temporal and spatial dynamics of seagrass
1020 landscapes using time-series remote sensing. *Estuarine, Coastal and Shelf Science*, 20, 42–53, 2013.
- 1021 Mandanici, E. and Bitelli, G.: Preliminary Comparison of Sentinel-2 and Landsat 8 Imagery for a Combined Use.
1022 *Remote Sensing*, 8, 1014, 2016. DOI:10.3390/rs8121014., 2016.
- 1023 Manevski, K., Manakos, I., Petropoulos, G. P. and Kalaitzidis, C.: Discrimination of common Mediterranean plant
1024 species using field Spectroradiometry. *Int. J. of Applied Earth Observation and Geoinformation*, 13, 922–933,
1025 2011.
- 1026 Marcello, J., Eugenio, F., Martín, J. and Marqués, F.: Seabed Mapping in Coastal Shallow Waters Using High
1027 Resolution Multispectral and Hyperspectral Imagery. *Remote Sensing*, 10, 1208. DOI:10.3390/rs10081208, 2018.
- 1028 Markham, B., Barsi, J., Kvaran, G., Ong, L., Kaita, E., Biggar, S., Czapla-Myers, J., Mishra, N. and Helder, D.:
1029 Landsat-8 Operational Land Imager Radiometric Calibration and Stability. *Remote Sensing*, 6(12), 12275-12308.
1030 <https://doi.org/10.3390/rs61212275>, 2014.
- 1031 Markham, B., Jenstrom, D., Masek, J. G., Dabney, P., Pedelty, J. A., Barsi, J.A. and Montanaro, M.: Landsat 9: Status
1032 and plans. In *Earth Observing Systems XXI; International Society for Optics and Photonics: San Diego, CA, USA;*
1033 *Volume 9972*, p. 99720G, 2016.
- 1034 Mcfeeters, S. K.: The use of the normalized difference water index (NDWI) in the delineation of open water features.
1035 *Int. Journal of Remote Sensing*, 17, 1425-1432, 1996.
- 1036 Meehan, A. J., Williams, R. J. and Watford, F. A.: Detecting Trends in Seagrass Abundance Using Aerial Photograph
1037 Interpretation: Problems Arising with the Evolution of Mapping Methods. *Estuaries*, 28(3), 462-472, 2005.
- 1038 Mount, R. E.: Rapid monitoring of extent and condition of seagrass habitats with aerial photography “mega-quadrats”.
1039 *Journal of Spatial Science*, 52 (1), 105-119, 2007.
- 1040 Morrison, M. A., Lowe, M. L., Grant, C. M., Smith, P. J., Carbines, G., Reed, J., Bury, S. J. and Brown, J. (2014)
1041 Seagrass meadows as biodiversity and productivity hotspots. *New Zealand Aquatic Environment and Biodiversity*,
1042 Report No. 137, 151 pages. <http://www.mpi.govt.nz/news-resources/publications.aspx>, 2014.
- 1043 Mumby, P. J., Green, E. P., Edwards, A. J. and Clark, C. D.: Measurement of Seagrass Standing Crop using Satellite
1044 and Digital Airborne Remote Sensing. *Marine Ecology Progress Series*, 159, 51-60, 1997.

- 1045 NASA (2014) Landsat-8 Instruments. Available online (accessed on 18 March 2021):
1046 http://www.nasa.gov/mission_pages/landsat/spacecraft/index.html, 2014.
- 1047 NASA: Landsat-9 Mission Details. Available online (accessed on 18 March 2021).
1048 <https://landsat.gsfc.nasa.gov/landsat-9/landsat-9-mission-details/>, 2019.
- 1049 NASA: Landsat-9 overview, continuity the legacy - 2021 and beyond. <https://landsat.gsfc.nasa.gov/landsat-9/landsat-9-overview>, 2021.
1050
- 1051 Naser, H.: Human Impacts on Marine Biodiversity: Macro-benthos in Bahrain, Arabian Gulf. Chapter 7 (pp. 109-126)
1052 in “The Importance of Biological Interactions in the Study of Biodiversity. Edited by J. LÃ³pez-Pujol, ISBN: 978-
1053 953-307-751-2. Published by InTech, 390 pp, 2011
- 1054 Neckles, H. A., Kopp, B. S., Peterson, B. J. and Pooler, P. S.: Integrating Scales of Seagrass Monitoring to Meet
1055 Conservation Needs. *Estuaries and Coasts*, 35(1), 23-46, 2012.
- 1056 Novak, A. B and Short, F. T.: Submerged Aquatic Vegetation: Seagrasses. *Encyclopedia of Natural Resources*, 9
1057 pages. DOI: 10.1081/E-ENRW-120047540, 2014.
- 1058 Onuf, C. P.: Seagrasses, dredging and light in Laguna Madre, Texas, U.S.A.: *Estuarine, Coastal and Shelf Science*,
1059 39, 75-91, 1994.
- 1060 Orth, R. J., Carruthers, T. J. B., Dennison, W. C., Duarte, C. M., Fourqurean, J. W., Heck, K. L., Hughes, A. R.,
1061 Kendrick, G. A., Kenworthy, W. J., Olyarnik, S. Short, F. T., Waycott, M. and Williams, S. L.: A Global Crisis
1062 for Seagrass Ecosystems. *Bioscience*, 56(12), 987–996. [https://doi.org/10.1641/0006-3568\(2006\)56\[987:AGCFSE\]2.0.CO;2](https://doi.org/10.1641/0006-3568(2006)56[987:AGCFSE]2.0.CO;2), 2006.
1063
- 1064 Pasqualini, V., Pergent-Martini, C., Pergent, G., Agreil, M., Skoufas, G., Sourbes, L. and Tsirika, A.: Use of SPOT 5
1065 for mapping seagrasses: An application to *Posidonia oceanica*. *Remote Sensing of Environment*, 94(1), 39-45,
1066 2005.
- 1067 Peneva, E., Griffith, J. A. and Carter, G. A.: Seagrass mapping in the northern Gulf of Mexico using airborne
1068 hyperspectral imagery: a comparison of classification methods. *Journal of Coastal Research*, 24(4), 850–856, 2008.
- 1069 Perez, D., Islam, K., Hill, V., Zimmerman, R., Schaeffer, B., Shen, Y. and Li, J.: Quantifying Seagrass Distribution
1070 in Coastal Water with Deep Learning Models. *Remote Sensing*, 12, 1581. DOI:10.3390/rs12101581, 2020.
- 1071 Peterson, B. J. and Fourqurean, J. W.: Large-scale patterns in seagrass (*Thalassia testudinum*) demographics in south
1072 Florida. *Limnology and Oceanography*, 46(5), 1077-1090, 2001.
- 1073 Phinn, S., Roelfsema, C., Dekker, A., Brando, V. and Anstee, J.: Mapping seagrass species, cover and biomass in
1074 shallow waters: An assessment of satellite multispectral and airborne hyper-spectral imaging systems in Moreton
1075 Bay (Australia). *Remote Sensing of Environment*, 112(8), 3413-3425, 2008.
- 1076 Preen, A.: Distribution, abundance and conservation status of dugongs and dolphins in the southern and western
1077 Arabian Gulf. *Biological Conservation*, 118(2), 205-218, 2004.
- 1078 Pu, R., Bell, S., Baggett, L., Meyer, C. and Zhao, Y.: Discrimination of Seagrass Species and Cover Classes with *in*
1079 *situ* Hyperspectral Data. *Journal of Coastal Research*, 28(6),1330-1344, 2012.
- 1080 Richardson, A. J. and Wiegand, C. L.: Distinguishing vegetation from soil background information. *Photogrammetric*
1081 *Engineering and Remote Sensing*, 43(12), 1541-1552, 1977.

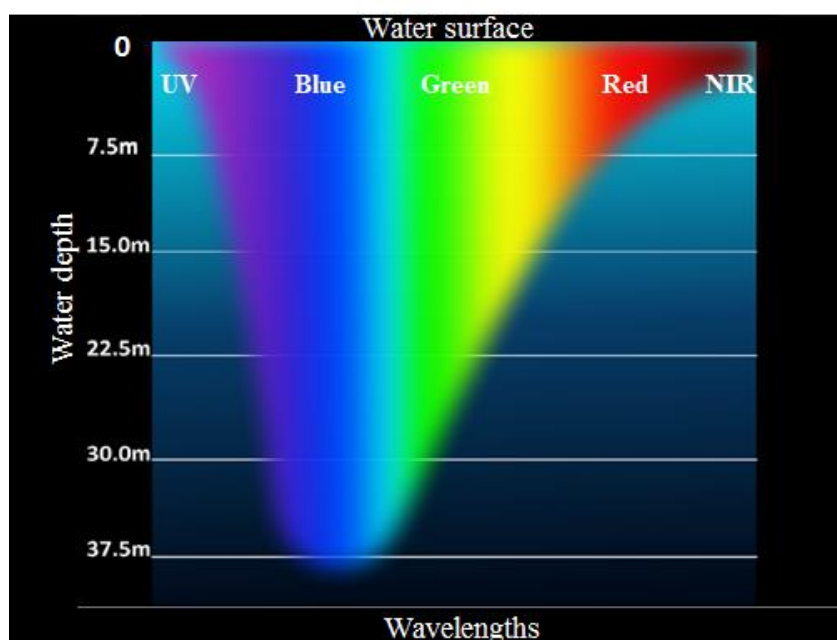
- 1082 Roelfsema, C. M., Lyons, M., Kovacs, E. M., Maxwell, P., Saunders, M. I., Samper-Villarreal, J. and Phinn, S. R.:
1083 Multi-temporal mapping of seagrass cover, species and biomass: A semi-automated object based image analysis
1084 approach. *Remote Sensing of Environment*, 150, 172–187, 2014.
- 1085 Roelfsema, C. M., Phinn, S. R., Udy, N. and Maxwell, P.: An integrated field and remote sensing approach for
1086 mapping seagrass cover, Moreton Bay, Australia. *Journal of Spatial Science*, 54(1), 45–62.
1087 <https://doi.org/10.1080/14498596.2009.9635166>, 2009.
- 1088 Rouse, J. W., Haas, R. W., Schell, J. A., Deering, D. W., Harlan, J. C. (1974) Monitoring the vernal advancement and
1089 retrogradation (Greenwave effect) of natural vegetation. NASA/GSFC Type-III Final Report, Greenbelt,
1090 Maryland, U.S.A., 164 pp, 1974.
- 1091 Roy, D. P., Li, J., Zhang, H. K., Yan, L., Huang, H. and Li, Z.: Examination of Sentinel-2A multi-spectral instrument
1092 (MSI) reflectance anisotropy and the suitability of a general method to normalize MSI reflectance to nadir BRDF
1093 adjusted reflectance. *Remote Sensing of Environment*, 199, 25-38. <https://doi.org/10.1016/j.rse.2017.06.019>,
1094 2017.
- 1095 Roy, D., Zhang, H., Ju, J., Gomez-Dans, J., Lewis, P., Schaaf, C., Sun, Q., Li, J., Huang, H. and Kovalskyy, V.: A
1096 general method to normalize Landsat reflectance data to nadir BRDF adjusted reflectance. *Remote Sensing of*
1097 *Environment*, 176, 255–271. <https://doi.org/10.1016/j.rse.2016.01.023>, 2016.
- 1098 Roy, D. P., Wulder, M. A., Loveland, T. R., Woodcock, C. E., Allen, R. G., Anderson, M. C., Helder, D., Irons, J. R.,
1099 Johnson, D. M., Kennedy, R., Scambos, T. A., Schaaf, C. B., Schott, J. R., Sheng, Y., Vermote, E. F., Belward, A.
1100 S., Bindschadler, R., Cohen, W. B., Gao, F., Hipple, J. D., Hostert, P., Huntington, J., Justice, C. O., Kilic, A.,
1101 Kovalskyy, V., Lee, Z. P., Lyburner, L., Masek, J. G., McCorkel, J., Shuai, Y., Trezza, R., Vogelmann, J.,
1102 Wynne, R. H. and Zhu, Z.: Landsat-8: science and product vision for terrestrial global change research. *Remote*
1103 *Sensing of Environment*, 145, 154–172. <https://doi.org/10.1016/j.rse.2014.02.001>, 2014.
- 1104 Saarman, E., Gleason, M., Ugoretz, J., Airamé, S., Carr, M., Fox, E., Frimodig, A., Mason, T. and Vasques, J.: The
1105 role of science in supporting marine protected area network planning and design in California, *Ocean and Coastal*
1106 *Management*, 74, 45-56. <https://doi.org/10.1016/j.ocecoaman.2012.08.021>, 2013.
- 1107 Sandmeier, St., Muller, Ch., Hosgood, B. and Andreoli, G.: Sensitivity Analysis and quality Assessment of Laboratory
1108 BRDF Data. *Remote Sensing of Environment*, 64, 176-191, 1998.
- 1109 Short, F. T. and Wyllie-Echeverria, S.: Natural and humaninduced disturbance of seagrasses. *Environ. Conserv.*, 23,
1110 17-27, 1996.
- 1111 Short, F. T. and Coles, R.: *Global Seagrass Research Methods*. Elsevier Publishing, The Netherlands, 482 pp, 2001.
- 1112 Short, F. T., Polidoro, B., Livingstone, S. R., Carpenter, K. E., Bandeira, S., Bujang, J. S., Calumpang, H. P.,
1113 Carruthers, T. J. B., Coles, R. G., Dennison, W. C., Erfemeijer, P. L. A., Fortes, M. D., Freeman, A. S., Jagtap,
1114 T. G., Kamal-Abu-Hena, M., Kendrick, G. A., Kenworthy, W. J., La-Nafie, Y. A., Nasution, I. M., Orth, R. J.,
1115 Prathep, A., Sanciangco, J. C., Tussenbroek, B. V., Vergara, S. G., Waycott, M. W. and Zieman, J. C.: Extinction
1116 risk assessment of the world's seagrass species. *Biological Conservation*, 144(7), 1961–1971.
1117 <https://doi.org/10.1016/j.biocon.2011.04.010>, 2011.

- 1118 Silva, T. S. F., Costa, M. P. F., Melack, J. M., and Novo, E. M. L. M.: Remote sensing of aquatic vegetation: Theory
1119 and applications. *Environmental Monitoring and Assessment*, 140(1-3), 131-145. [https://doi.org/10.1007/s10661-](https://doi.org/10.1007/s10661-007-9855-3)
1120 [007-9855-3](https://doi.org/10.1007/s10661-007-9855-3), 2008.
- 1121 Skakun, S., Roger, J.-C., Vermote, E. F., Masek, J. G. and Justice, C. O.: Automatic sub-pixel co-registration of
1122 Landsat-8 Operational Land Imager and Sentinel-2A Multi-Spectral Instrument images using phase correlation
1123 and machine learning based mapping. *Int. J. of Digital Earth*, 10(12), 1253-1269.
1124 <http://dx.doi.org/10.1080/17538947.2017.1304586>, 2017.
- 1125 Slater, P. N.: *Remote Sensing - Optics and Optical System*. Addison-Wesley, reading, MA, 575 pp. 1980.
- 1126 Teillet, P. M. and Santer, R.: Terrain Elevation and Sensor Altitude Dependence in a Semi-Analytical Atmospheric
1127 Code". *Canadian J. of Remote Sensing*, 17, 36-44, 1991.
- 1128 Thakur, Y. et al.: Sea Turtles. Chapter 9, pp. 165–177. In *Marine Environment and Resources of Abu Dhabi*, edited
1129 by T.Z. Al-Abdessalam, published by Environment Agency of Abu-Dhabi, UAE, 255 pp, 2007.
- 1130 Thorhaug, A., Richardson, A. D. and Berlyn, G. P.: Spectral reflectance of the seagrasses: *Thalassia testudinum*,
1131 *Halodule wrightii*, *Syringodium filiforme* and five marine algae. *Int. Journal of Remote Sensing*, 28(7), 1487–
1132 1501, 2007.
- 1133 Traganos, D.: Development of seagrass monitoring techniques using remote sensing data. PhD Thesis, Osnabrück
1134 University, Osnabrück in Lower Saxony, Germany, 199 pp, 2020.
- 1135 Uhrin, A. V. and Townsend, P. H.: Improved Seagrass Mapping Using Linear Spectral Unmixing of Aerial
1136 Photographs. *Estuarine, Coastal and Shelf Science*, 171, 11-22, 2016.
- 1137 Umamaheswari, R., Ramachandran, S. and Nobi, E. P.: Mapping the extend of seagrass meadows of Gulf of Mannar
1138 Biosphere Reserve, India using IRS ID satellite imagery. *Int. Journal of Biodiversity and Conservation*, 1(5), 187-
1139 193, 2009.
- 1140 Van-Der-Meera, F.: Analysis of spectral absorption features in hyperspectral imagery. *Int. J. Appl. Earth Observation*
1141 and *Geoinformation*, 5, 55–68, 2004.
- 1142 Van-der-Werff, H. and Van-der-Meer, F.: Sentinel-2A MSI and Landsat 8 OLI Provide Data Continuity for Geological
1143 Remote Sensing. *Remote Sensing*, 8, 883. <https://doi.org/10.3390/rs8110883>, 2016.
- 1144 Vermote, E., Justice, C., Claverie, M. and Franch, B.: Preliminary analysis of the performance of the Landsat 8/OLI
1145 land surface reflectance product. *Remote Sensing of Environment*, 185(2), 46–56.
1146 DOI: 10.1016/j.rse.2016.04.008, 2016.
- 1147 Villa, P., Bresciani, M., Braga, F. and Bolpagni, R.: Comparative Assessment of Broadband Vegetation Indices over
1148 Aquatic Vegetation. *IEEE Journal of Selected Topics in Applied Earth Observations and Remote Sensing*, 7(7),
1149 3117-3127, 2014.
- 1150 Villa, P., Mariano Bresciani, M., Braga, F. and Bolpagni, R.: Mapping Aquatic Vegetation through Remote Sensing
1151 Data: A Comparison of Vegetation Indices Performances. 6th EARSeL Workshop on Remote S. of the Coastal
1152 Zone, 7-8 June 2013, Matera, Italy, pp. 10-15, 2013.

- 1153 Wabnitz, C. C., Andréfouët, S., Torres-Pulliza, D., Muller-Karger, F. E. and Kramer, P. A.: Regional-scale seagrass
1154 habitat mapping in the Wider Caribbean region using Landsat sensors: Applications to conservation and ecology.
1155 *Remote Sensing of Environment*, 12(8), 3455-3467, 2008.
- 1156 Warren, C., Dupont, J., Abdel-Moati, M., Hobeichi, S., Palandro, D. and Purkis, S.: Remote sensing of Qatar nearshore
1157 habitats with perspectives for coastal management. *Marine Pollution Bulletin*, 105(2), 641-653.
1158 <https://doi.org/10.1016/j.marpolbul.2015.11.036>, 2016.
- 1159 Waycott, M., Duarte, C. M., Carruthers, T. J. B., Orth, R. J., Dennison, W. C., Olyarnik, S., Calladine, A.,
1160 Fourqurean, J. W., Heck Jr., K. L., Hughes, A. R., Kendrick, G. A., Kenworthy, W. J., Short, F. T. and Williams,
1161 S. L.: Accelerating loss of seagrasses across the globe threatens coastal ecosystems. *PNAS* July 28,
1162 2009; 106 (30) 12377-12381; www.pnas.org/cgi/doi/10.1073/pnas.0905620106, 2009.
- 1163 Wicaksono, P. and Hafizt, M.: Mapping Seagrass from Space: Addressing the Complexity of Seagrass LAI Mapping,
1164 *European Journal of Remote Sensing*, 46(1), 18-39. <http://dx.doi.org/10.5721/EuJRS20134602>, 2013.
- 1165 Wicaksono, P., Fauzan, M. A., Kumara, I. S. W., Yogyantoro, R. N., Lazuardi, W. and Zhafarina, Z.: Analysis of
1166 reflectance spectra of tropical seagrass species and their value for mapping using multispectral satellite images.
1167 *Int. Journal of Remote Sensing*, 40(23), 8955-8977. DOI: 10.1080/01431161.2019.1624866, 2019.
- 1168 Wicaksono, P., Kumara, I. S., Kamal, M., Fauzan, A. M., Zhafarina, Z., Nurswantoro, D. A. and Yogyantoro, R. N.:
1169 Multispectral Resampling of Seagrass Species Spectra: WorldView-2, Quickbird, Sentinel-2A, ASTER VNIR,
1170 and Landsat 8 OLI. The 5th Geoinformation Science Symposium 2017 (GSS 2017). IOP Conf. Series: Earth and
1171 Environmental Science, 98(2017), 012039. DOI:10.1088/1755-1315/98/1/012039, 2017.
- 1172 Willmott, C.J.: Some comments on the evaluation of model performance. *Bull. Am. Meteorol. Soc.*, 63, 1309-1313,
1173 1982.
- 1174 Wood, J. S.: Hyperspectral analysis of seagrass in Redfish Bay, Texas. Ph.D. Thesis, Texas A&M University-Corpus
1175 Christi, Corpus Christi, Texas (USA), 141 pp, 2012.
- 1176 Wulder, M. A., Hilker, T., White, J. C., Coops, N. C., Masek, J. G., Pflugmacher, D. and Crevier, Y.: Virtual
1177 constellations for global terrestrial monitoring. *Remote Sensing of Environment*, 170, 62-76.
1178 <https://doi.org/10.1016/j.rse.2015.09.001>, 2015.
- 1179 Yan, L., Roy, D.P., Li, Z., Zhang, H.K. and Huang, H.: Sentinel-2A multi-temporal misregistration characterization
1180 and an orbit-based sub-pixel registration methodology. *Remote Sensing of Environment*, 215, 495-506.
1181 <https://doi.org/10.1016/j.rse.2018.04.021>, 2018.
- 1182 Yang, D. and Yang, C.: Seagrass Distribution in China with Satellite Remote Sensing. Chapter 4 in *Remote Sensing*
1183 *of Planet Earth*, edited by Yann Chemin, pp. 75-94. ISBN: 978-953-307-919-6, InTech. Available from:
1184 [http://www.intechopen.com/books/remote-sensing-of-planet-earth/seagrass-distribution-in-china-with-](http://www.intechopen.com/books/remote-sensing-of-planet-earth/seagrass-distribution-in-china-with-remotesensing)
1185 [remotesensing](http://www.intechopen.com/books/remote-sensing-of-planet-earth/seagrass-distribution-in-china-with-remotesensing), 2012.
- 1186 Yang, D. and Yang, C.: Detection of seagrass distribution changes from 1991 to 2006 in Xincun Bay, Hainan, with
1187 satellite remote sensing. *Sensors*, 9(2), 830-844, 2009.
- 1188 Zhang, H. K. and Roy, D. P.: Computationally inexpensive Landsat-8 operational land imager (OLI) pan-sharpening.
1189 *Remote Sensing*, 8 (3), 180, 2016.

- 1190 Zhang, H. K., Roy, D. P., Yan, L., Li, Z., Huang, H., Vermote, E., Skakun, S. and Roger, J. C.: Characterization of
 1191 Sentinel-2A and Landsat-8 top of atmosphere, surface, and nadir BRDF adjusted reflectance and NDVI
 1192 differences. Remote Sensing of Environment, 215, 482-494. <https://doi.org/10.1016/j.rse.2018.04.031>, 2018.
- 1193 Zhao, D., Lv, M., Jiang, H., Cai, Y., Xu, D. and An, S.: Spatio-Temporal Variability of Aquatic Vegetation in Taihu
 1194 Lake over the Past 30 Years. PLoS ONE, 8(6), 6–12. <https://doi.org/10.1371/journal.pone.0066365>, 2013.
- 1195 Zoffoli, M. L., Gernez, P., Rosa, P., Le-Bris, A., Brando, V. E., Barille, A.-L., Harin, N., Peters, S., Poser, K., Spaias,
 1196 L., Peralta, G. and Barille, L.: Sentinel-2 remote sensing of *Zostera noltei*-dominated intertidal seagrass meadows.
 1197 Remote Sensing of Environment, 251, 112020, 2020.
- 1198 Zorrilla, N. A., Vantrepotte, V., Ngoc, D.-D., Huybrechts, N. and Gardel, A.: Automated SWIR based empirical sun
 1199 glint correction of Landsat 8-OLI data over coastal turbid water. Optics Express, 27(8), A294-A318.
 1200 <https://doi.org/10.1364/OE.27.00A294>, 2019.

1201
 1202
 1203
 1204
 1205



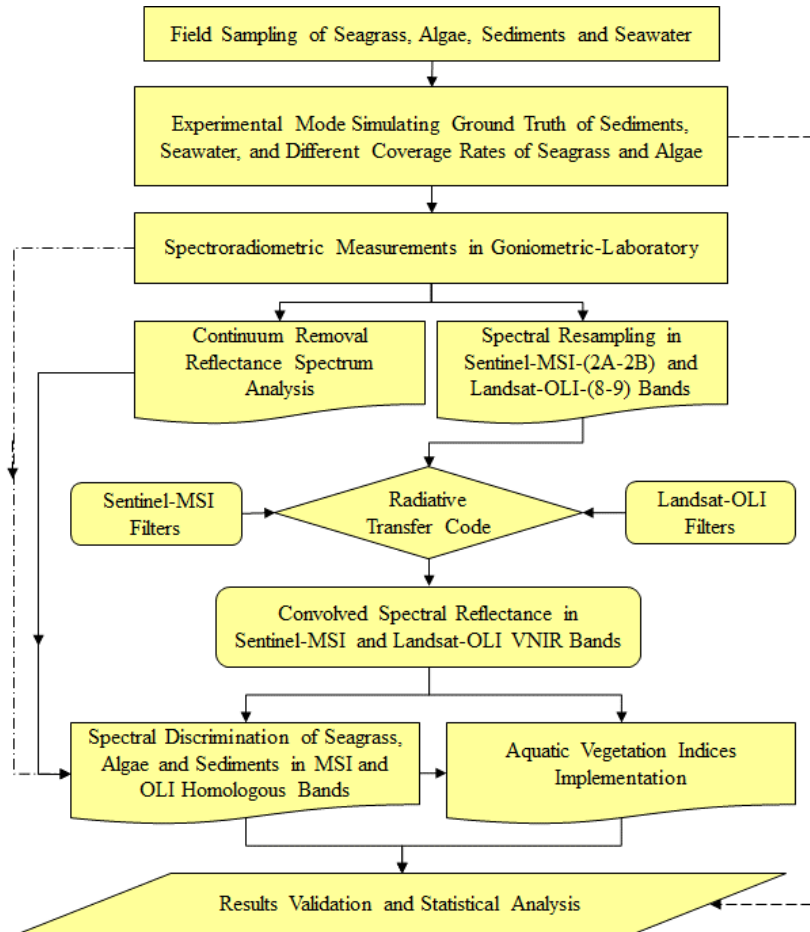
1206
 1207 **Figure 1.** Vertical penetration of electromagnetic spectrum in shallow water (adapted from: Morris, 2019),
 1208 https://commons.wikimedia.org/wiki/Category:Visible_spectrum_illustrations)

1209
 1210
 1211
 1212

1213

1214

1215



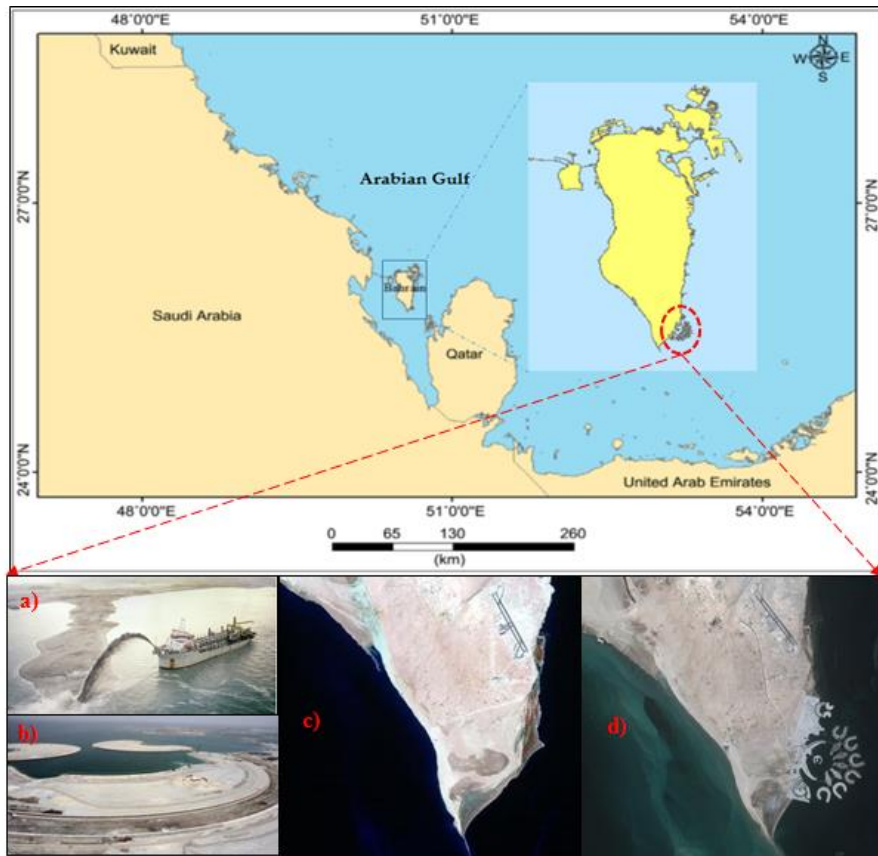
1216

1217 **Figure 2.** Methodology Flowchart

1218

1219

1220



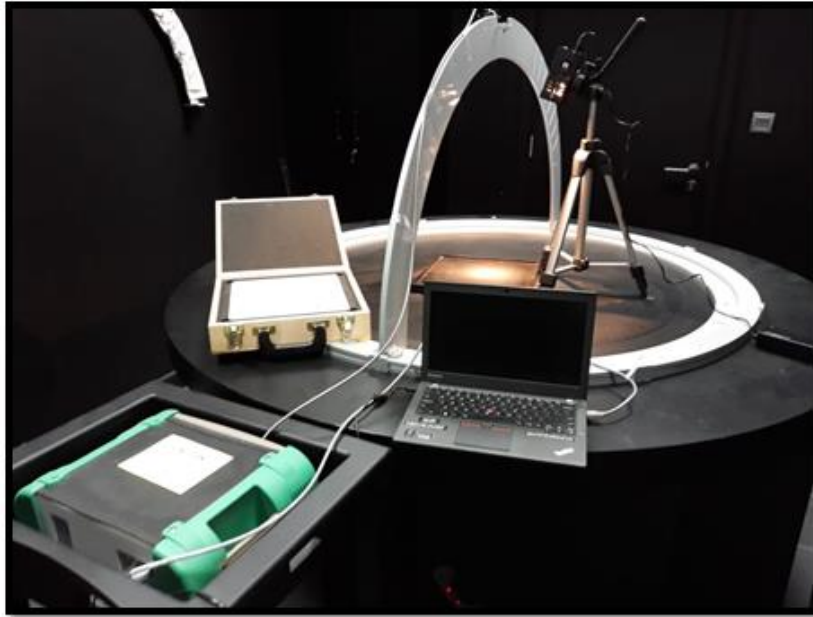
1221
 1222 **Figure 3.** Study site (Kingdom of Bahrain), photos illustrating dredging operations (a and b), and satellite images of
 1223 the south part of Bahrain before (c) and after (d) artificial islands construction.

1224



1225
 1226 **Figure 4.** Diver for sampling operation (a), and underwater photos of the considered seagrass and algae species: HU
 1227 (b), HS (c), BA (d), GA (e), and bright sediments (f).

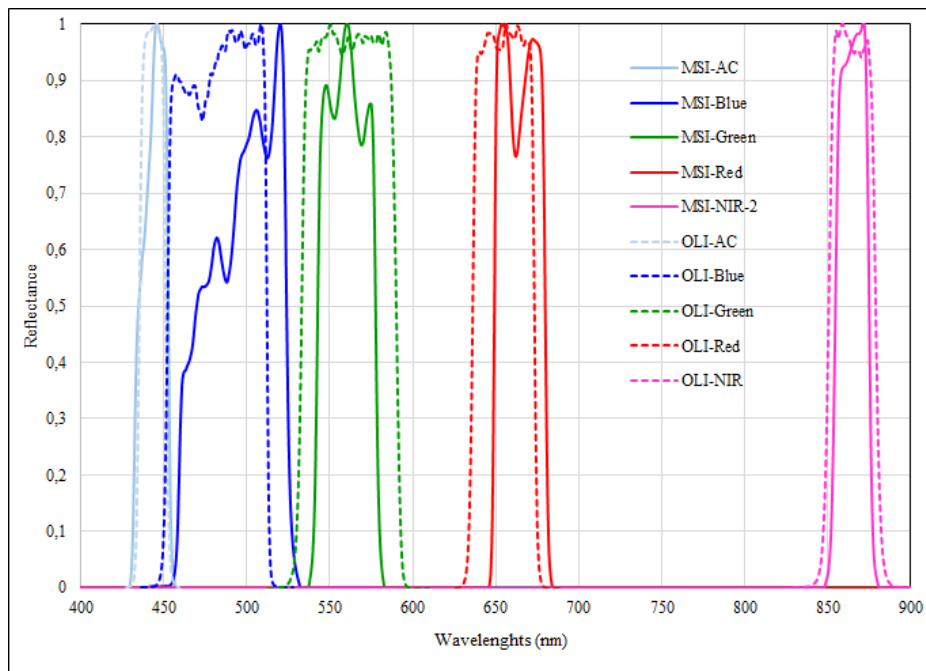
1228



1229

1230 **Figure 5:** Dark Goniometric-Laboratory for ASD measurements.

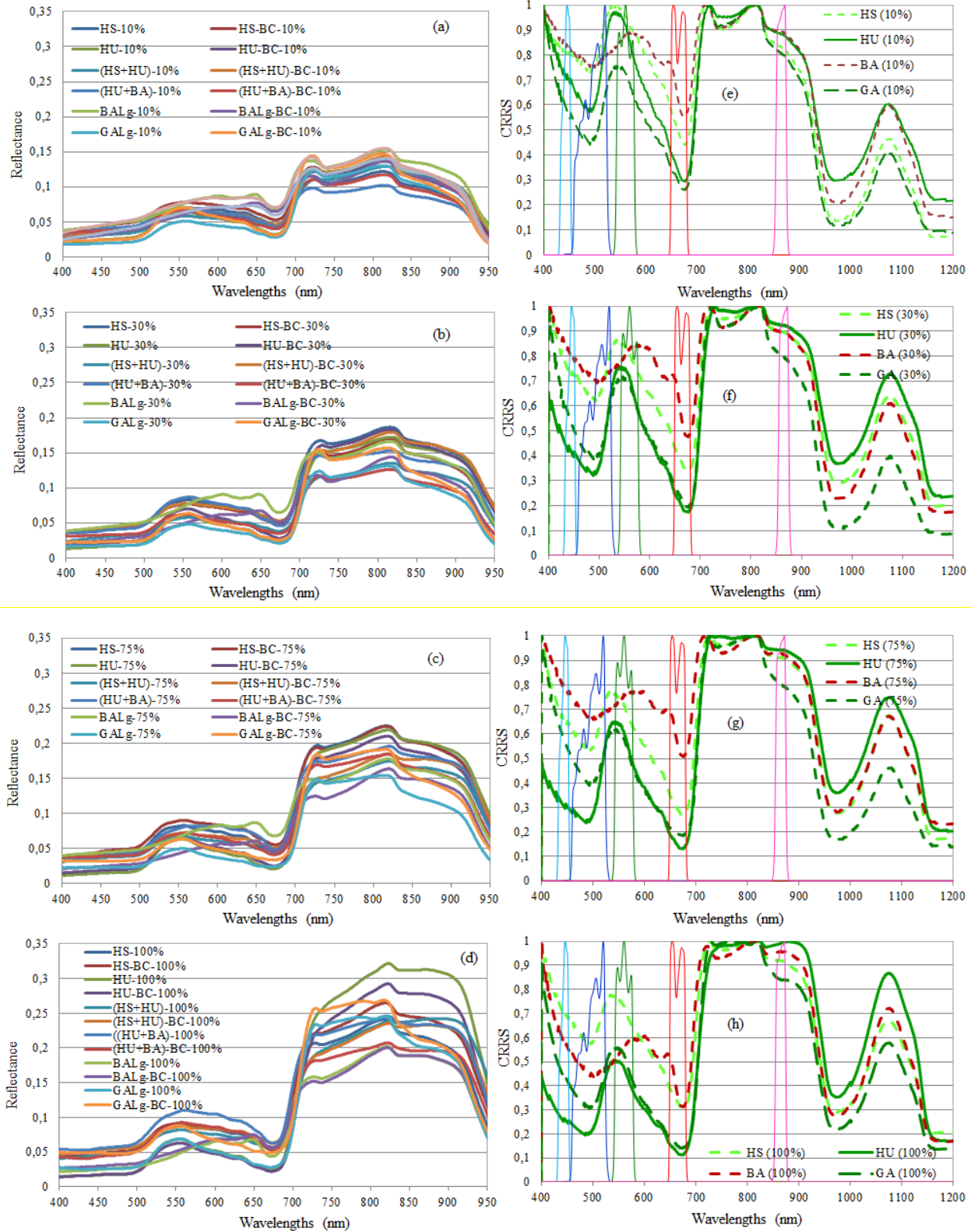
1231



1232

1233 **Figure 6.** Sentinel-MSI and Landsat-OLI relative spectral response profiles characterizing the filters of each spectral
1234 band in the VNIR.

1235



1236

1237

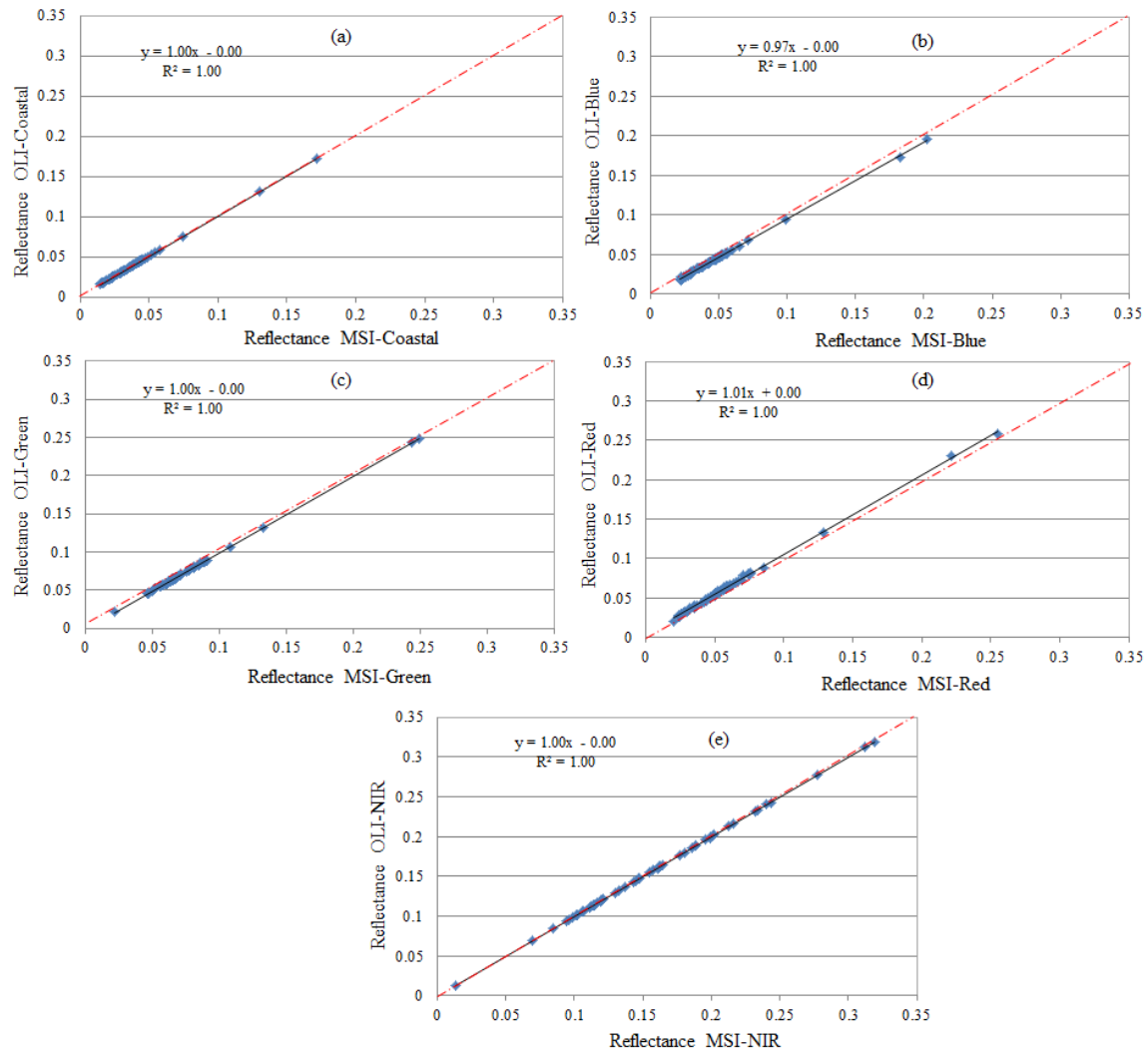
1238 **Figure 7.** Spectral signatures of seagrass and algae samples at different coverage rates (a: 10%, b: 30%, c: 75%, and

1239 d: 100%) and their CRRS transformations.

1240

1241

1242



1243

1244 **Figure 8.** Scatter-plots of reflectances sampled and convolved in MSI and OLI homologous spectral bands.

1245

1246

1247

1248

1249

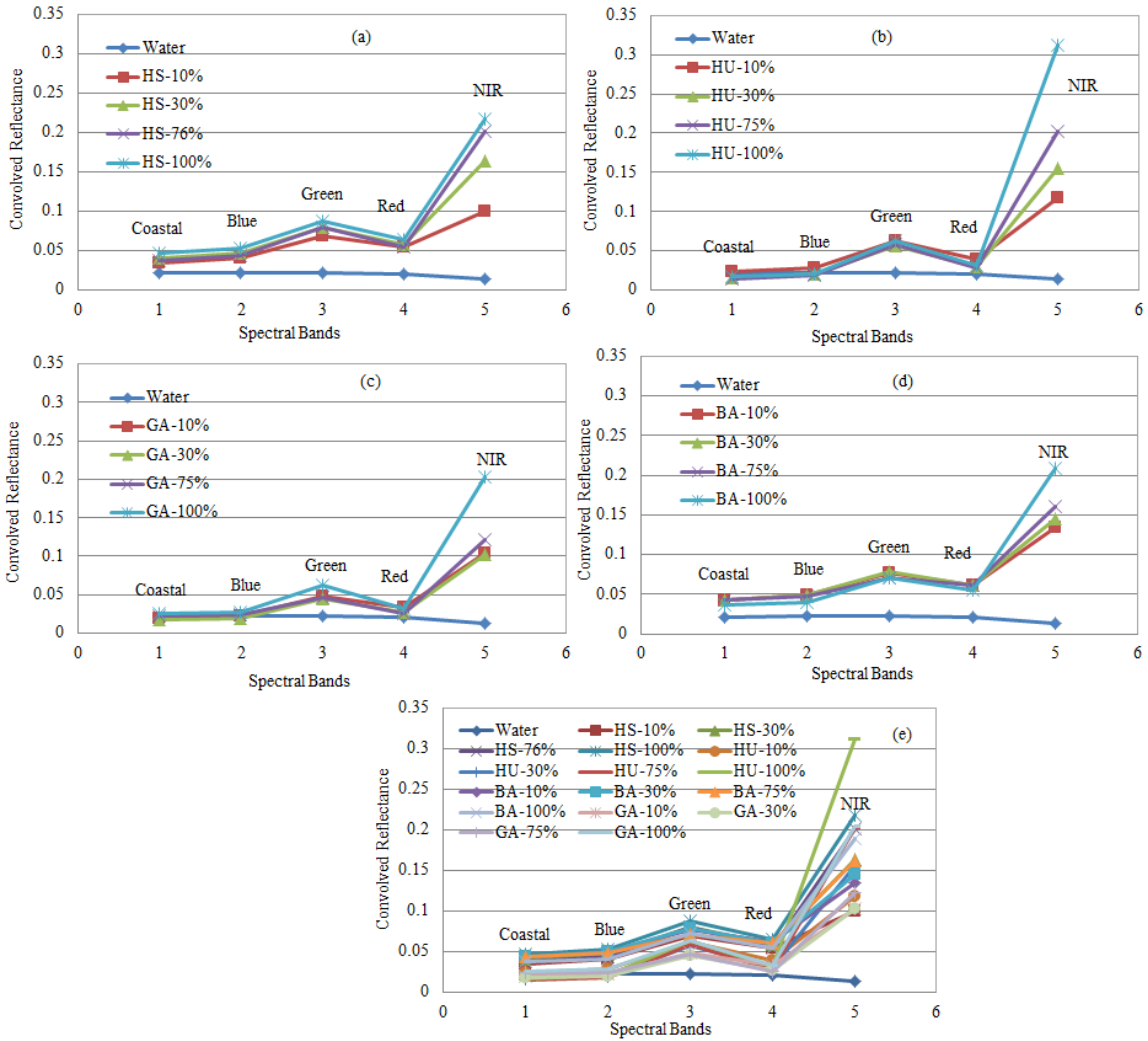
1250

1251

1252

1253

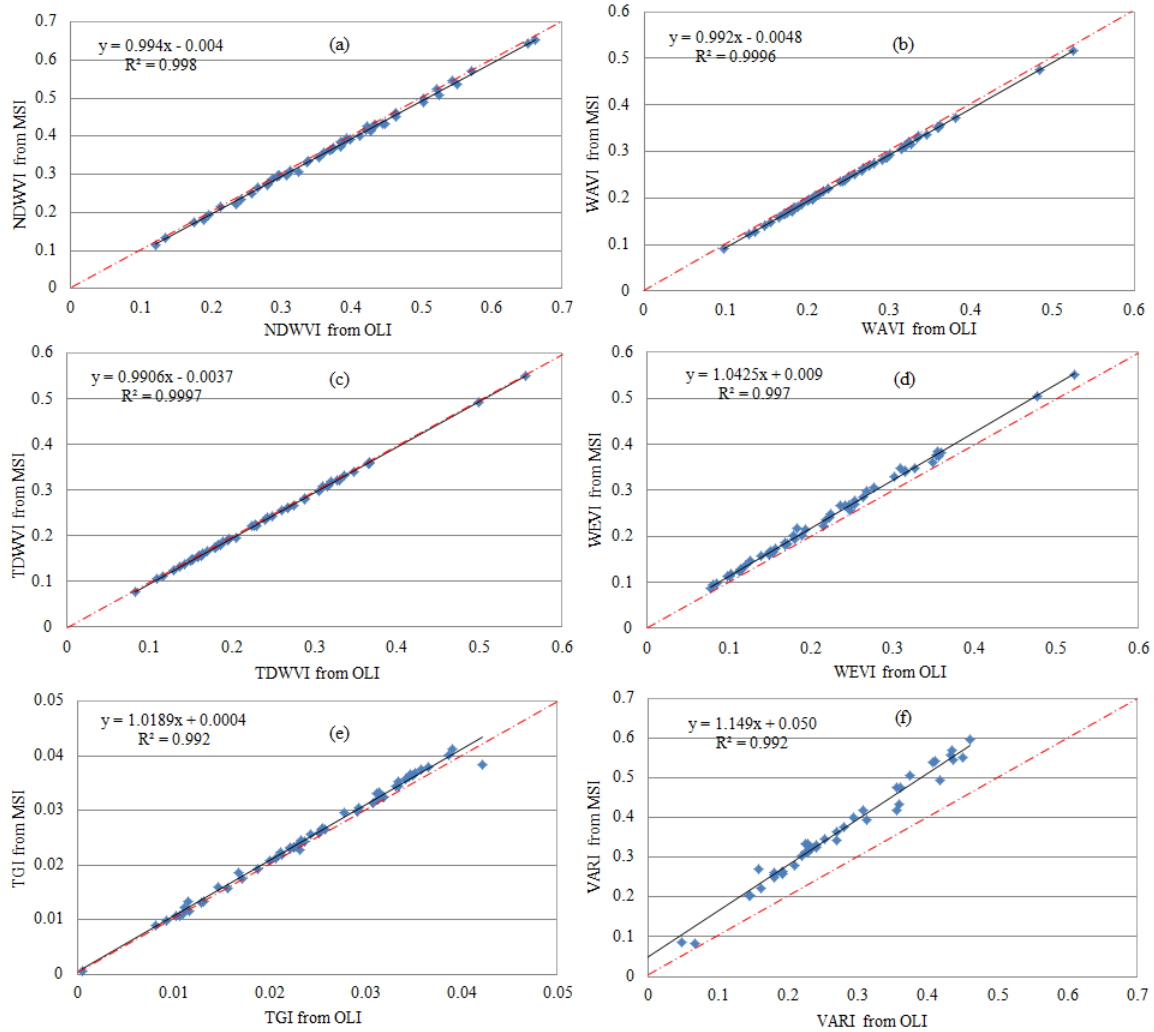
1254



1255

1256 **Figure 9.** Seagrass, algae, and seawater reflectances resampled and convolved in VNIR bands of Sentinel-MSI (or
 1257 Landsat-OLI): HS (a), HU (b), GA (c), BA (d), and all samples (e).

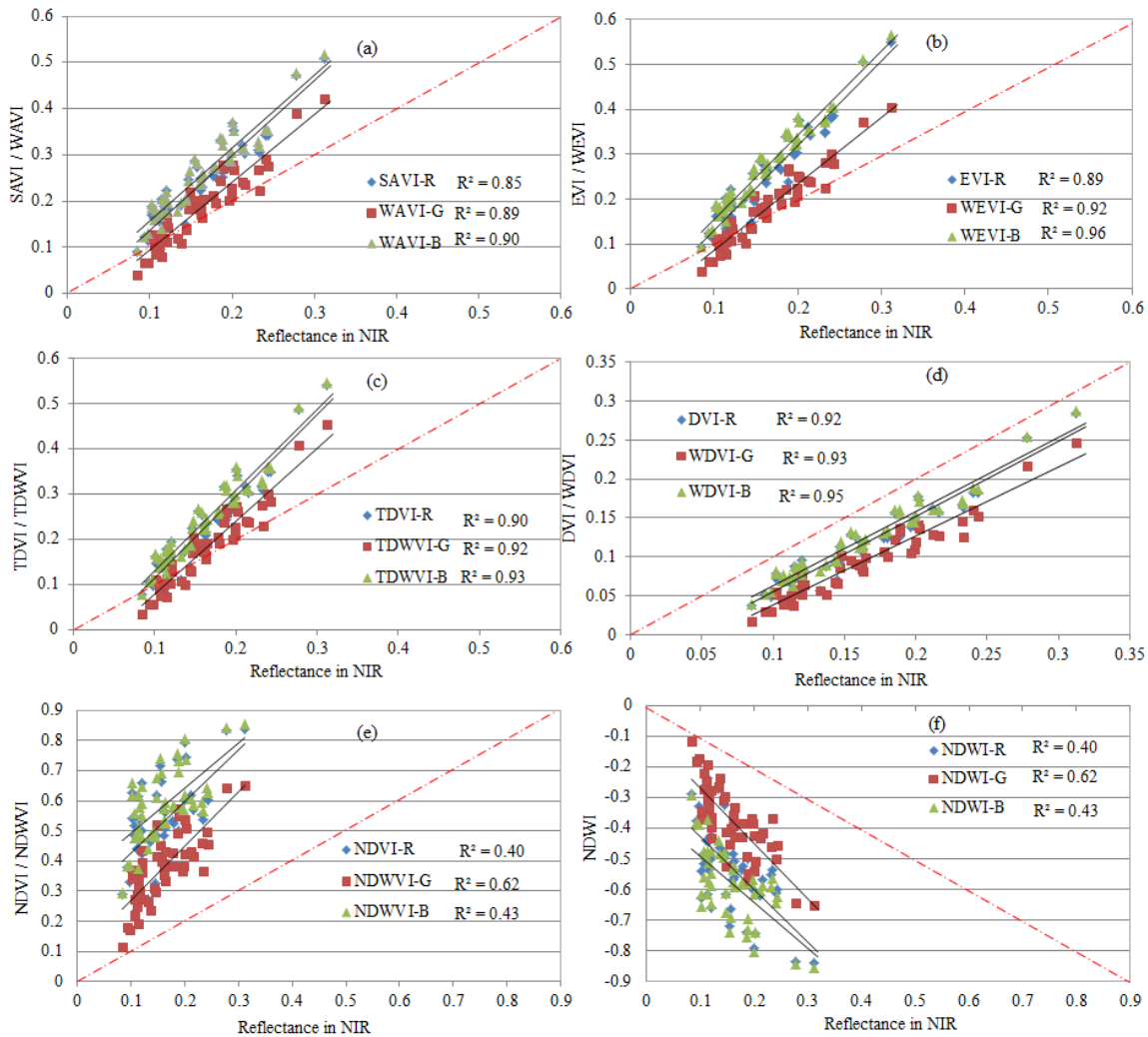
1258



1259

1260 **Figure 10.** Scatter-plots of homologous WVI derived from MSI and OLI simulated data.

1261



1262
 1263 **Figure 11.** Linear regressions ($p < 0.05$) between WVI and reflectance in NIR considering all samples, and integrating
 1264 the red, green, and blue bands.
 1265

1266 **Table 1.** The Sentinel-MSI and Landsat-OLI effective bandwidths and characteristics (λ = wavelength, SNR = signal
 1267 to noise ratio, $L_{ref}(\lambda)$ = reference radiance, $E_0(\lambda)$ = Extra-atmospheric irradiance,).

| Spectral Bands | Sentinel-MSI | | | | | Landsat-OLI | | | | |
|----------------|-----------------------|----------------------|----------------|-----|---|-----------------------|----------------------|----------------|-----|----------------------------------|
| | λ Centre (nm) | $\Delta\lambda$ (nm) | Pixel Size (m) | SNR | $L_{ref}(\lambda)$ ($w/m^2/Sr/\mu m$) | λ Centre (nm) | $\Delta\lambda$ (nm) | Pixel Size (m) | SNR | $E_0(\lambda)$ ($w/m^2/\mu m$) |
| Coastal | 443 | 20 | 60 | 129 | 129 | 443 | 16 | 30 | 130 | 1895.6 |
| Blue | 490 | 65 | 10 | 154 | 128 | 482 | 60 | 30 | 130 | 2004.6 |
| Green | 560 | 35 | 10 | 168 | 128 | 561 | 57 | 30 | 100 | 1820.7 |
| Red | 655 | 30 | 10 | 142 | 108 | 655 | 38 | 30 | 90 | 1549.4 |
| NIR-2 | 865 | 20 | 20 | 72 | 52.5 | 865 | 28 | 30 | 90 | 951.2 |
| SWIR-1 | 1609 | 85 | 20 | 100 | 4 | 1609 | 85 | 30 | 100 | 247.6 |
| SWIR-2 | 2201 | 187 | 20 | 100 | 1.5 | 2201 | 187 | 30 | 100 | 85.5 |

1268

1269

1270
 1271 **Table 2.** R^2 ($p < 0.05$) between vegetation indices integrating red, blue, and green bands and the reflectances in NIR
 1272 for all considered samples, and the RMSD between indices derived from MSI and OLI sensors data.

| Index | Used band | R^2 | RMSD* in % | Index | Used band | R^2 | RMSD* in % | Index | Used band | R^2 | RMSD* in % |
|-------|-----------|-------------|---------------|-----------|-----------|-------------|---------------|-------|-----------|-------------|---------------|
| NDVI | R | 0.40 | 1.0 | TDVI | R | 0.90 | 0.3 | DVI | R | 0.92 | 0.2 |
| | G | 0.63 | 0.5 | | G | 0.92 | 0.2 | | G | 0.93 | 0.1 |
| | B | 0.43 | 1.0 | | B | 0.93 | 0.2 | | B | 0.95 | 0.1 |
| SAVI | R | 0.85 | 0.3 | EVI | R | 0.89 | 0.9 | NDWI | R | 0.40 | 1.0 |
| | G | 0.89 | 0.2 | | G | 0.92 | 0.3 | | G | 0.63 | 0.5 |
| | B | 0.90 | 0.2 | | B | 0.96 | 0.3 | | B | 0.43 | 1.0 |
| TGI | | 0.20 | 0.1 | Diff(G-B) | | 0.63 | 0.1 | VARI | | 0.63 | 3.0 |

1273 * is the RMSD between indices derived from MSI and OLI simulated data. The bold type highlight the significant R^2 .

1274

1275